# An Efficient SSP-based Methodology for Assessing Climate Risks of a Large Credit Portfolio

Florian Bourgey, Emmanuel Gobet, Ying Jiao

# An Efficient Shared Socioeconomic Pathways-Based Methodology for Assessing Climate Risks of a Large Credit Portfolio

Florian Bourgey[1], Emmanuel Gobet[2*], Ying Jiao[3]

[1]Quantitative Research, Bloomberg L.P., 731 Lexington Ave, New York, 10022, NY, USA.
[2]Centre de Mathématiques Appliquées, CNRS, Ecole Polytechnique, Institut Polytechnique de Paris, Palaiseau, France.
[3]ISFA, Laboratoire SAF, Université Claude Bernard - Lyon 1, Lyon, France.

*Corresponding author(s). E-mail(s): emmanuel.gobet@polytechnique.edu;
Contributing authors: fbourgey@bloomberg.net; ying.jiao@univ-lyon1.fr;

**Abstract**

We examine climate-related exposure within a large credit portfolio, addressing transition and physical risks. We design a modeling methodology that begins with the Shared Socioeconomic Pathways (SSP) scenarios and ends with describing the losses of a portfolio of obligors. The SSP scenarios impact the physical risk of each obligor via a DICE-inspired damage function and their transition risk through production, requiring optimal adjustment. To achieve optimal production, the obligor optimizes various energy sources to align its greenhouse gas (GHG) emission trajectories with SSP objectives, while accounting for uncertainties in consumption trajectories. Ultimately, we obtain a Gaussian factor model whose dimension is of the order of the number of obligors. Two efficient dimension reduction methods (Polynomial Chaos Expansion and Principal Component Analysis) provide a fast and accurate method for analyzing credit portfolio losses.

**Keywords:** Climate Risks, Transitions Risks, Physical Risks, Credit Risk, Polynomial Chaos Expansion, Principal Component Analysis, Shared Socioeconomic Pathways, Optimal Production Profit.

**MSC Classification:** 91G60 , 91G40 , 91B38 , 86A08

# 1 Introduction

***Climate risk and financial impact.***

Facing the challenges of climate change, financial institutions are encouraged to shift their activities and investments toward a low-carbon economy. Under the Network for Greening the Financial System (NGFS), an increasing number of international banks have committed to the agreements made at the Conference of the Parties (COP 24) in Katowice in 2018, aiming to align their portfolios with the $CO_2$ trajectories of the Paris Agreement. In other words, banks should incorporate the impact of climate change into the management of their asset portfolios. Notably, measuring and assessing the potential consequences of climate risks has become a key issue for financial institutions.

According to the Intergovernmental Panel on Climate Change (IPCC), $CO_2$ and, more generally, greenhouse gas (GHG) emissions are among the main causes of global temperature increase. To achieve the idealized objective of limiting average warming to no higher than $1.5^o$C, the IPCC summarizes [19] different potential macro-scenarios called Representative Concentration Pathways (RCP) to indicate possible GHG abatement scenarios. Based on more detailed socioeconomic criteria and factors, many other scenarios, known as Shared Socioeconomic Pathways (SSPs), have been proposed in the scientific literature, e.g., [27, 35]. These scenarios allow firms in different sectors and countries to anticipate and implement their mitigation strategy.

Climate risks in finance encompass two primary categories: physical and transition risks, as discussed in [9] and [2]. Physical risks entail immediate losses to companies due to shocks, especially as the severity and frequency of events like floods, heatwaves, and wildfires increase in extreme climate scenarios. Transition risks, on the other hand, result from firms shifting toward low-carbon production methods, profoundly influencing their future trajectory and impacting financial institutions and investors in the market. Modeling both risks remains a complex task with many uncertainties and limitations, but it is crucial for financial institutions granting loans to economic companies (obligors) to consider the transmission channels of climate-related risk drivers in the credit risk analysis of their portfolio. For the insurance sector, climate change, particularly physical risks, can significantly affect an insurer's balance sheet, especially in non-life insurance, and lead to substantial consequences for insurance companies providing financial protection against climate-related loss events (see, e.g., [12]). The impact of both transition and physical risks on the insurance sector is a highly topical issue; see the recent works of [14, 33] regarding non-life insurers and their credit risk.

Our study focuses on selected SSP scenarios, which describe future paths of GHG emissions across various sectors and temperature trajectories. We downscale these scenarios to individual obligors to model their adaptations (transition risks) and their impacts on physical risks. Subsequently, we aggregate this modeling at the credit portfolio level. The primary quantity of interest is the portfolio cumulative loss defined below in (1). The challenge we undertake is twofold: first, to design a robust and meaningful model; second, to efficiently and accurately solve and sample it, given the large number of obligors in the portfolio.

***Literature on large portfolios and credit analysis.***

Financial institutions manage large portfolios consisting of $n$ obligors, where $n$ can be on the order of hundreds of thousands for major international banks. The cumulative loss is typically expressed as

$$\mathcal{L} = \sum_{i=1}^{n} \Lambda^i \times \mathbf{1}_{\{X^i \leq d^i\}} \tag{1}$$

where $\Lambda^i$ (resp., $d^i$) represents the loss given default multiplied by the exposure at default (resp., the default barrier) of the $i$th obligor, $X^i$ is the obligor's default-relevant variable, which also characterizes the dependence between obligors through correlated random factors. Modeling the marginal distributions of $X^i$ and their dependence is crucial. In the current work, we explicitly model $X^i$ and $d^i$ in terms of the related SSP.
*In the credit-risk literature neglecting climate risks*, there exist two main approaches to describing the dependence of credit portfolios: the so-called bottom-up and top-down models. In the first approach, we start with the marginal distribution of each default time. Then, we specify the correlation structure, frequently utilizing copula models. For a comprehensive survey, refer to McNeil and Frey [28]. In the second approach, we focus directly on the cumulative loss process for credit portfolios to overcome the computational burden associated with portfolio size (see, e.g., [4]). In the first approach, when the size of a credit portfolio is very large, advanced numerical methods must be used as any naive Monte Carlo simulation becomes too time-consuming. Moreover, standard market models often impose a simplified dependence structure to facilitate computation. In factor models such as the Gaussian copula model, all obligors in the portfolio are correlated through one or several common macroeconomic or financial risk factors. Conditionally on these common factors, the default of the underlying companies is independent, as their heterogeneous factors are. A typical example is the one-factor Gaussian copula model of Li [26], where the loss is expressed as (1). In this model, $X^i = \rho^i Z + \sqrt{1-(\rho^i)^2}\varepsilon^i$ with $Z$ and $\varepsilon^i$ being independent standard normal random variables, and $\rho^i \in (-1,1)$ being the correlation parameter. The default barrier $d^i$ is deterministic.

We can also consider a multivariate default intensity model, generalizing the standard one-dimensional Cox model [23]. For a fixed horizon time $T > 0$, let $X^i = \int_0^T (\lambda_s + \lambda_s^i)\,\mathrm{d}s$ where $\lambda$ and $\lambda^i$ are non-negative processes representing the default intensity induced by common and individual risk factors. The default barrier $d^i$ is an independent exponential random variable. For other classical factor models in credit risk modeling and analysis, refer to [40] and [16].
*In the credit-risk literature accounting for climate risks*, the authors of [13] consider a multi-factor model called the Climate-Extended Risk Model (CERM) with several common risk factors, i.e., $Z$ is a centered Gaussian random vector with a given correlation matrix. Our contribution is different as we consider a bottom-up modeling approach and additionally provide an efficient computational scheme to analyze the cumulative loss (1). To integrate the impact of climate risk into credit-sensitive firms and asset portfolios, [24] develops a structural model for defaultable bonds of companies exposed to transition risks. Unlike [24], which focuses on a single obligor, we

model the credit risk of a large portfolio and also account for physical risks. Climate disaster-related events, such as Hurricane Harvey, have been incorporated using jump-diffusion processes to measure the impact of physical risks on the default probability of the housing sector, as demonstrated in [25]. In [10], the authors propose an integrated assessment of energy transition risk that links future energy scenarios to a structural economic model (Merton's model). This methodology is applied to electric utility companies located in the 28 European Union countries, focusing on the financial impacts of decarbonization policies. Another closely related work is [22], where the authors apply an asset-and-liability model to analyze the impact of carbon costs on default probabilities. They consider various fuel mix plans and carbon price scenarios, with a particular focus on Eskom, South Africa's state-owned utility. Unlike our approach, these two papers do not consider physical risk and focus solely on electric utilities. In contrast to [25], our work focuses on a portfolio of obligors, accounting for dependence, and incorporates both physical and transition risks. Furthermore, adjustments to default probabilities and bond portfolio valuations are derived under various climate scenarios, based on the technological profiles of firms facing transition risks, as outlined in [3]. As a difference with [3], we focus on the credit risk of the portfolio rather than individual obligors. Additionally, our approach integrates both physical and transition risks into the modeling, and addresses related computational challenges.

***Contributions of our paper.***

We propose a multi-default model that accounts for both transition and physical risks. Our contributions encompass three key aspects. Our comprehensive approach to modeling and computational methods is summarized in Figure 1. This diagram is included for pedagogical clarity: it provides the reader with an overview of the methodology developed and the main quantitative results obtained.

Firstly, on the modeling front and following the approach of [5], we start from a target emission scenario, such as one of the SSPs, and derive the obligor's transition efforts and strategies by considering a mix of different energy types, their respective emission factors, and associated costs; see Theorems 1, 2 and 3. These factors directly impact the obligor's production methods and credit quality. The correlation structure among obligors is modeled by introducing common systemic factors, akin to market factor models. This approach differs from [5], where the focus is on a unique energy source and a cost function for a single obligor.

Secondly, in Section 3, we incorporate the projected costs associated with future physical risks that affect the obligor's overall value. This estimation draws on historical cost data and a modeling approach inspired by the Dynamic Integrated Model of Climate and Economy (DICE), reminiscent of Nordhaus' work [30, Eq. 5 p.10]. This approach acknowledges the inertia between GHG emissions and their subsequent effects on physical risks. Overall, our model offers a transparent mechanism for tracing how climate risks influence the creditworthiness of individual obligors. The marginal default probability for each obligor can be inferred using a bottom-up credit modeling approach. This is an additional extension to [5], which did not model physical risk.

Thirdly, we turn to computing credit risk metrics for large-scale portfolios using a top-down framework. Drawing inspiration from [6], we introduce an efficient

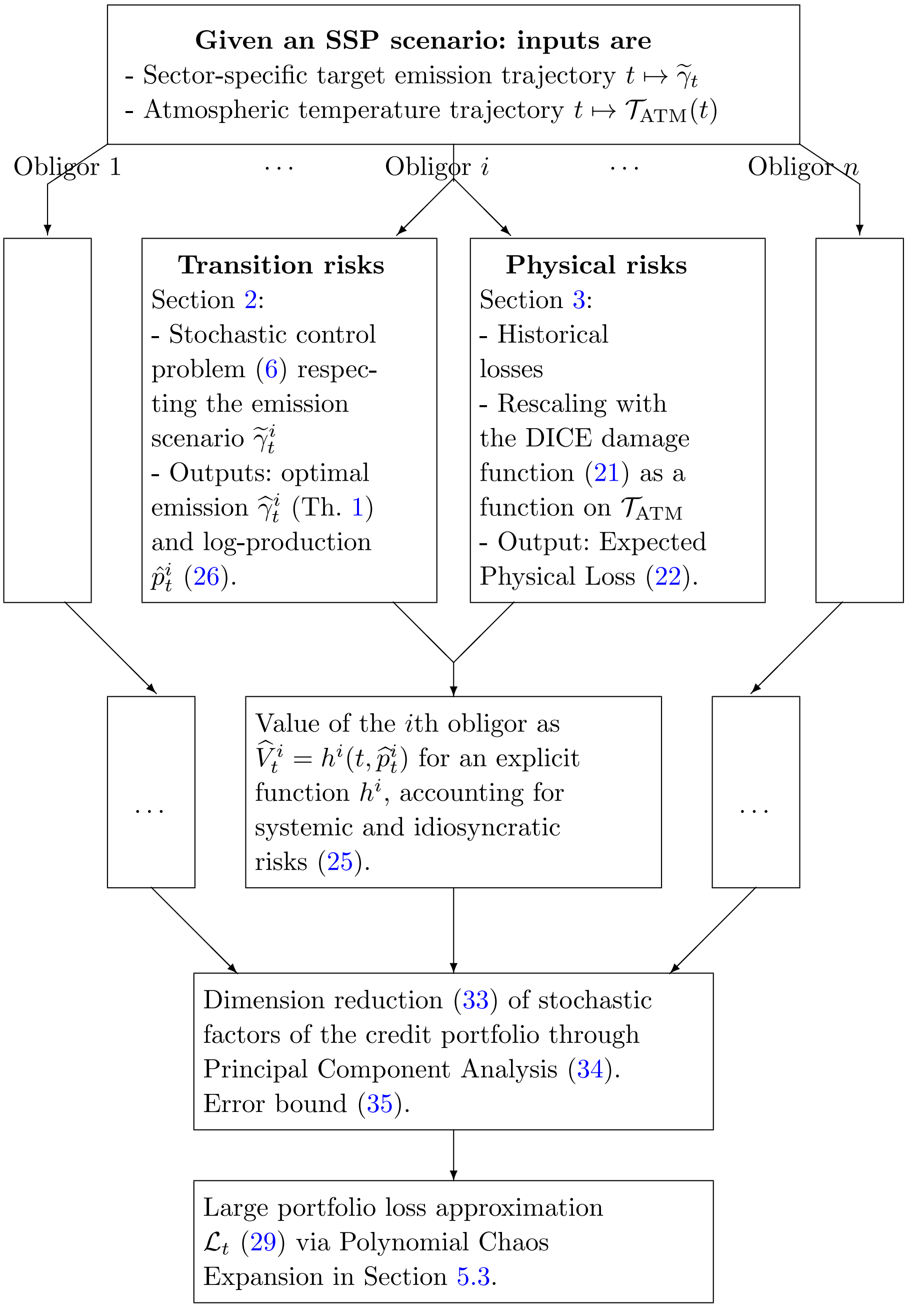


**Fig. 1** Diagram illustrating the analysis of the problem.

numerical method based on Polynomial Chaos Expansions (PCE) for evaluating cumulative losses, see Section 5.3. However, our approach stands out by integrating dimension-reduction techniques specifically tailored to address climate risk.

As mentioned earlier, the correlation structure among obligors is established through a common systemic risk factor. We propose a method to reduce both the common and all idiosyncratic risk factors (amounting to $n+1$ factors) to just $2+\frac{1}{2}(M+1)(M+2)$ factors, where $M$ is limited to a few units. This reduction is substantiated quantitatively through two main approaches: a) an analysis of eigenvalues via Principal Component Analysis (PCA), yielding two significant factors (see Section 5.2 and Proposition 5 for an $L^1$ error estimate), and b) a Polynomial Chaos Expansion applied to the limited systemic factors to perform a Gaussian approximation with $\frac{1}{2}(M+1)(M+2)$ terms. Additionally, we provide an error estimation for the truncated losses based on findings from [6, Theorems 2.6-7]. The improvement is significant especially for $n$ large, as discussed in Subsection 5.3. Our method has shown both accuracy and speed in practical applications, supported by numerical experiments.

The remainder of the paper is structured as follows. Section 2 addresses transition risk, deriving optimal emission strategies for an obligor navigating low-carbon mitigation transitions. Section 3 examines various potential physical risks and their impact on the obligor's value process. In Section 4, we quantify the combined impact of transition and physical risks on the obligor's credit quality, providing a semi-explicit formula for default probability in a special setting. Section 5 focuses on aggregating credit risks and calculating cumulative losses for large portfolios, introducing efficient numerical methods for computation. Technical details are deferred to the Appendix.

# 2 Modeling the transition risk of each portfolio obligor

## 2.1 Overview of the approach

We consider a portfolio composed of $n \in \mathbb{N}^*$ companies whose production depends on their GHG emission levels measured in carbon dioxide equivalent $\mathtt{CO_2e}$ where $\mathtt{CO_2e}$ means that all GHG emissions have been converted into $\mathtt{CO_2}$ emissions. To allow comparison of the global warming of different gases, climate scientists use global warming potential (GWP) factors to convert one unit of a particular GHG to one unit of $\mathtt{CO_2}$. For example, methane $\mathtt{CH_4}$ has a GWP of about 27-30 over 100 years. Note that GHGs differ in their radiative efficiency (ability to absorb energy) and their lifetime (how long they stay in the atmosphere), see [34, Table 2.14] for a detailed table of these different GHG characteristics.

The companies aim to optimize their emission strategies following a low-carbon mitigation transition. Specifically, the $i$th obligor solves the infinite-horizon optimization problem

$$\mathcal{J}^i\left(\gamma^i_\bullet\right) = \mathbb{E}\left[\int_0^\infty e^{-rt}\left(\pi^i(P^i_t) - \mathcal{C}^i(\gamma^i_{\bullet,t}) - \ell^i_1(\gamma^i_{\bullet,t}) + \ell^i_2(\gamma^i_{\bullet,t})\right)\mathrm{d}t\right] \tag{2}$$

where

- $P^i$ is the obligor's production assumed to depend on time and to be stochastic as it accounts for the demand uncertainty in goods. It will be modeled using the Stochastic Differential Equation (4) which will be detailed later. The production dynamics depends also on the energy power coming from different energy sources $\mathsf{e} \in \mathscr{E}^i$ where $\mathscr{E}^i$ is the set of all of the energy sources available to the $i$th obligor. The energy power is proportional to the vector of GHG emissions $\gamma^i_\bullet := (\gamma_\mathsf{e})_{\mathsf{e}\in\mathscr{E}^i}$. We refer to Subsection 2.2 for details, in particular equation (4) which describes how $\gamma^i_\bullet := (\gamma_\mathsf{e})_{\mathsf{e}\in\mathscr{E}^i}$ affects $P^i$.
- $\pi^i$ is a profit function and $r > 0$ is a discount factor.
- $\mathcal{C}^i(\gamma^i_\bullet)$ represents the cost of purchasing these different primary energies, see (3).
- National and international authorities penalize (resp., reward) companies emitting above (resp., below) an emission target, see below. This is encoded in the term $\ell^i_1(\gamma^i_\bullet)$ (resp., $\ell^i_2(\gamma^i_\bullet)$), see Examples 1 and 2.

Comparing (2) with [5, Eq. 3], we note again that different energy sources are considered through the term $\gamma^i_\bullet := (\gamma_\mathsf{e})_{\mathsf{e}\in\mathscr{E}^i}$ and an additional reward term $\ell_2$ is included; this is a significant difference with [5] as it allows for more realism in terms of adaptation policy.

In our model, we do not consider any carbon compensation or offset, and we ignore carbon permits that could be traded in carbon markets. This extension is left to further research.

In the end, the optimal emission policy for the $i$th obligor is

$$\widehat{\gamma}^i_\bullet = \arg\sup_{\gamma^i_\bullet \in \mathcal{A}^i} \mathcal{J}^i\left(\gamma^i_\bullet\right),$$

where $\mathcal{A}^i$ is the set of admissible emission policies for the $i$th obligor. In this simplified model, we assume that companies are correlated through a common market factor but they do not interact with each other through the drift coefficient.

Last, our approach for modeling production takes $\mathtt{CO_2e}$ emissions as inputs, while taking energy consumptions as inputs may initially appear more intuitive, given that these consumptions yield different $\mathtt{CO_2e}$ emissions. In fact, both approaches are equivalent because of the ratio $\theta^i_{\mathsf{e},t} > 0$. In our modeling, we prefer to focus on $\mathtt{CO_2e}$ emissions.

Below, we describe each step and establish that, under suitable model hypotheses, there exists a unique emission policy for each obligor.

## 2.2 Modeling the link between GHG emissions and production

***Energy sources: GHG emissions, emission factors, and cost.***

According to the U.S. Energy Information Administration (EIA)[1], the different energy sources used by the U.S. industrial sector are: natural gas, petroleum, electricity, renewable sources (mainly biomass), and coal. Depending on how and where these energy sources are produced, their climate impact and price are different. For example,

[1] https://www.eia.gov/energyexplained/use-of-energy/industry.php

most companies purchase electricity from electric utilities, independent power producers, or possibly produce electricity for their own use with solar panels. Electricity can be produced from nuclear energy (nuclear power plant), renewable energy (wind, hydroelectric power plant, photovoltaic), fossil energy (oil, coal-fired power plant) or a combination of nuclear/renewable/fossil energies. Depending on where the obligor operates and its choice of suppliers, the electricity might be produced from a different electric mix. To illustrate this, Table 1 shows an example of three different UK Electricity Suppliers as of 2022. Observe for example that electricity produced from nuclear energy (resp., gas) is 63.1% (resp., 15.1%) for EDF Energy and 7.0% (resp., 74.0%) for Utilita.

| Supplier | Coal | Gas | Nuclear | Renewable | Other | Emission factor ($\mathtt{kgCO_2e}$ per $\mathtt{kWh}$) |
|---|---|---|---|---|---|---|
| Utilita | 9.0 | 74.0 | 7.0 | 3.0 | 8.0 | 0.429 |
| e.on | 2.0 | 16.1 | 1.5 | 78.8 | 1.6 | 0.093 |
| EDF Energy | 1.6 | 15.1 | 63.1 | 19.0 | 1.2 | 0.082 |
| Bulb | 0 | 0 | 0 | 100.0 | 0 | $\approx 0$ |

**Table 1** Fuel Mix (in %) of some of the UK Domestic Electricity Suppliers as of 2022. Those values are taken from https://electricityinfo.org/fuel-mix-of-uk-domestic-electricity-suppliers/. We assume here that $\mathtt{1kgCO_2e} \approx \mathtt{1kgCO_2}$ for electricity production. Note that because of The Electricity (Fuel Mix Disclosure) Regulations Act of 2005, electric suppliers are obligated to provide details of the mix of fuels used to produce electricity https://www.legislation.gov.uk/uksi/2005/391/contents/made.

| Source of Energy | Emission factors ($\mathtt{kgCO_2e}$ per $\mathtt{kWh}$) |
|---|---|
| Electricity (Coal) | 0.820 |
| Electricity (Gas) | 0.490 |
| Electricity (Wind) | 0.011 |
| Electricity (Nuclear) | 0.012 |
| Electricity (Hydro) | 0.024 |
| Charcoal | 0.403 |
| Crude Oil | 0.264 |
| Natural Gas | 0.202 |

**Table 2** A few examples of emission factors. For the emission factors from electricity generation, we report the median values of the lifecycle emissions from [38, Table A.III.2]. For the others, we report the default emission factors of [15, Table 2.2]. We have used the conversion $\mathtt{1kg/TJ} = \frac{18}{5} \times 10^{-6} \times \mathtt{1kg/kWh}$ where $\mathtt{1TJ}$ is one tera joule. Those values are also reported at https://ourworldindata.org/grapher/carbon-dioxide-emissions-factor

The last column of Table 1 is the so-called emission factor (sometimes called emission intensity or carbon output rate)[2]. It quantifies how much GHG emissions (measured in $\mathtt{CO_2e}$) are released when consuming 1 $\mathtt{kWh}$ of a particular energy source $\mathtt{e}$. Examples of emissions factors are reported in Table 2. Observe that the emission

[2]terminology from https://ember-climate.org/insights/research/european-electricity-review-2022/ and https://www.eia.gov/tools/glossary/index.php?id=c

factor for electricity produced from coal is about $\frac{0.820}{0.012} \approx 68$ times higher than electricity produced from nuclear energy. Emission factors for world countries as of 2022 are reported in [18].

We also stress that countries have different energy mix profiles. For example, in Figure 2, we plot the energy mix for China, the USA, and France in 2022. The share of electricity produced from nuclear energy is 63% for France, 5% for China, 18% for the USA, while when produced from coal it is 1% for France, 61% for China, and 19% for the USA.

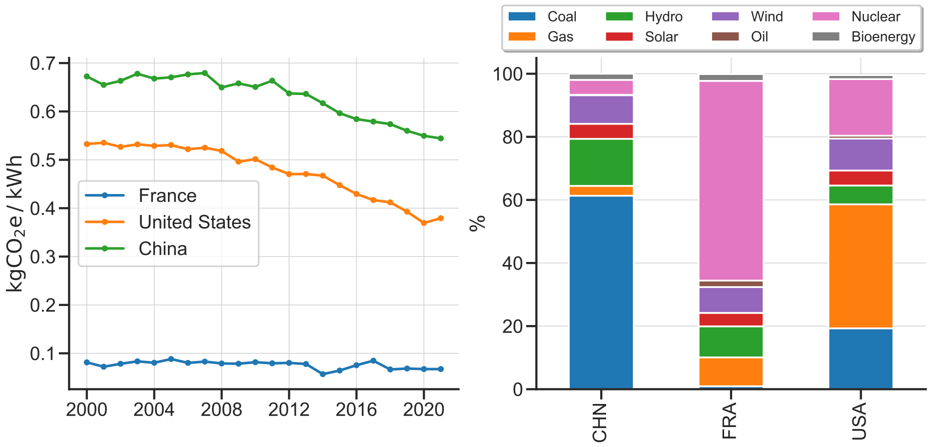


**Fig. 2** Left: Emission factors of electricity in `kgCO₂e/kWh` as a function of time for France, the USA, and China. Right: Bar plots of the electricity mix as of 2022 for the same countries. Data taken from [36].

***Notation.***

In our model, we denote by $\mathscr{E}^{\text{all}}$ the set of all possible energy sources[3] an obligor can use for its production:

$$\begin{aligned}\mathscr{E}^{\text{all}} := \big\{&\text{Coal consumption, Coal coke net imports, Petroleum consumption,}\\ &\text{Dry natural gas consumption, Nuclear electricity net generation,}\\ &\text{Hydroelectricity net generation, Geothermal electricity net generation,}\\ &\text{Solar thermal and photovoltaic electricity net generation,}\\ &\text{Wind electricity net generation, Electricity net imports, ...}\big\}.\end{aligned}$$

We let $\mathscr{E}^i \subseteq \mathscr{E}^{\text{all}}$ be the energy sources available to the $i$th obligor. Notice the dependence of $i$ for $\mathscr{E}^i$ as the set of all available energy sources might differ from one obligor to the other (different locations, different suppliers, etc). An obligor is unlikely to have access to all possible energy sources $\mathscr{E}^{\text{all}}$ and to use all available energy sources

[3] It corresponds to the list of energy sources for "Primary Energy Consumption" in the EIA's glossary https://www.eia.gov/tools/glossary.

$\mathscr{E}^i$. This fact will be materialized in the constraint set $\mathcal{G}^i$, see (8) in Subsection 2.3. We stress that we are not attempting to optimize the selection of energy sources $(\mathtt{e})_{\mathtt{e}\in\mathscr{E}^i}$, but rather to optimize the obligor's emissions $(\gamma_{\mathtt{e}})_{\mathtt{e}\in\mathscr{E}^i}$.

Two features characterize an energy source $\mathtt{e} \in \mathscr{E}^i$:

- the price $\alpha^i_{\mathtt{e},t} > 0$ per unit of e-energy consumed by the $i$th obligor at time $t$. The price may differ from one obligor to the other as it depends on the location of the obligor's offices, factories, and its access to related energy supply companies and their rates. We assume that the price is a deterministic function of time [4]. Its unit is USD/kWh. In Figure 3, we plot the yearly U.S. average prices of gasoline, gas, and electricity from 1978-79 to 2023.
- the power/$\mathtt{CO_2e}$ ratio $\theta^i_{\mathtt{e},t} > 0$. It corresponds to the average production rate for each energy e, i.e., the quotient of the total equivalent power production with respect to the equivalent $\mathtt{CO_2}$ emission from using e. Its unit is $\mathtt{kW/kgCO_2e}$. It equals the inverse of the emission factor (previously described), divided by one hour. These power/$\mathtt{CO_2e}$ ratios may depend on $i$ because companies may differ in their geographic zones and countries with different electricity mixes, as illustrated in Figure 2. We assume that each $t \mapsto \theta^i_{\mathtt{e},t}$ is a deterministic function of time.

For every obligor, there exists a trade-off between price and emission factor depending on how "green" the obligor is. An obligor might want to pay more for using "cleaner" energy sources. However, the obligor's probability of default could increase if the costs of fulfilling carbon obligations (e.g., through carbon pricing or sequestration) become too high. Conversely, successful mitigation strategies and efficient management of such obligations can help achieve financial net zero, as introduced in [20].

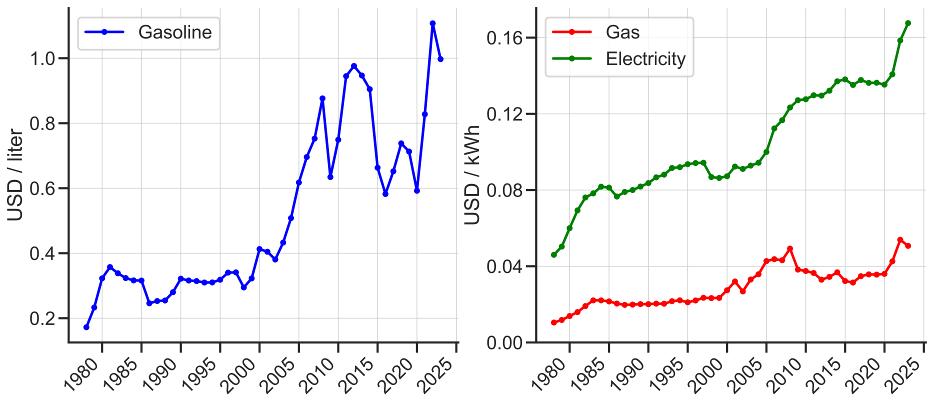


**Fig. 3** Left: Yearly US average price of Gasoline in USD/liter. Right: Yearly US average prices of household gas and electricity in USD/kWh. Source: U.S. Bureau of Labor Statistics.

We denote by $\gamma^i_{\bullet,t} := (\gamma^i_{\mathtt{e},t})_{\mathtt{e}\in\mathscr{E}^i}$ the vector of instantaneous GHG emissions for the $i$th obligor coming from each of the primary energy sources $\mathtt{e} \in \mathscr{E}^i$. Its unit is $\mathtt{kgCO_2e}$.

[4] Ideally, the price $\alpha_{\mathtt{e},t}$ should depend on the future scenario pathway considered. Electric price scenarios for some sectors are available in the AR6 database https://data.ene.iiasa.ac.at/ar6

With our notations, the instantaneous energy (in kWh) coming from e consumed during a small interval $[t, t + \mathrm{d}t]$ (in hours h) is then

$$\theta^i_{\mathtt{e},t} \times \gamma^i_{\mathtt{e},t} \ \mathrm{d}t.$$

The cost (in USD) of consuming such energy is

$$\alpha^i_{\mathtt{e},t} \times \theta^i_{\mathtt{e},t} \times \gamma^i_{\mathtt{e},t} \ \mathrm{d}t,$$

while the cost (in USD) of consuming energy coming from all sources $\mathtt{e} \in \mathscr{E}^i$ is

$$\sum_{\mathtt{e}\in\mathscr{E}^i} \alpha^i_{\mathtt{e},t} \times \theta^i_{\mathtt{e},t} \times \gamma^i_{\mathtt{e},t} \ \mathrm{d}t =: \alpha^{i,\theta}_{\bullet,t} \cdot \gamma^i_{\bullet,t} \ \mathrm{d}t$$

where we have introduced the short-hand notation

$$\alpha^{i,\theta}_{\bullet,t} := (\alpha^i_{\mathtt{e},t} \times \theta^i_{\mathtt{e},t})_{\mathtt{e}\in\mathscr{E}^i},$$

and $\cdot$ denotes the scalar product. In addition, to account for the limited amount of energy available at a given date, we add a quadratic term that captures the fact that marginal energy cost is increasing with the demand. Introducing the notations,

$$\beta^{i,\theta}_{\bullet,t} := \left(\beta^i_{\mathtt{e},t} \times (\theta^i_{\mathtt{e},t})^2\right)_{\mathtt{e}\in\mathscr{E}^i}, \qquad (\gamma^2)^i_{\bullet,t} := ((\gamma^i_{\mathtt{e},t})^2)_{\mathtt{e}\in\mathscr{E}^i},$$

the total energy cost over the interval $[t, t + \mathrm{d}t]$ writes as

$$\begin{aligned} \mathcal{C}^i(\gamma^i_{\bullet,t}) \ \mathrm{d}t &= \sum_{\mathtt{e}\in\mathscr{E}^i} \left(\alpha^i_{\mathtt{e},t} \times \left(\theta^i_{\mathtt{e},t} \times \gamma^i_{\mathtt{e},t}\right) + \beta^i_{\mathtt{e},t} \times \left(\theta^i_{\mathtt{e},t} \times \gamma^i_{\mathtt{e},t}\right)^2\right) \ \mathrm{d}t \\ &= \left(\alpha^{i,\theta}_{\bullet,t} \cdot \gamma^i_{\bullet,t} + \beta^{i,\theta}_{\bullet,t} \cdot (\gamma^2)^i_{\bullet,t}\right) \ \mathrm{d}t \end{aligned} \tag{3}$$

where $t \mapsto \alpha^i_{\mathtt{e},t}$ and $t \mapsto \beta^i_{\mathtt{e},t}$ (and thus $t \mapsto \alpha^{i,\theta}_{\mathtt{e},t}$ and $t \mapsto \beta^{i,\theta}_{\mathtt{e},t}$) are strictly positive and deterministic measurable functions of time for any $\mathtt{e} \in \mathscr{E}^i$. In the specific example of [5, Eq. 14], a single energy type was considered, and the total energy cost was entirely quadratic in the emissions. Here, we consider various types of energy and include a linear term in the emissions to model the cost in USD of consuming energies. An illustration on how obligor emissions may evolve with time is depicted later in Figure 5.

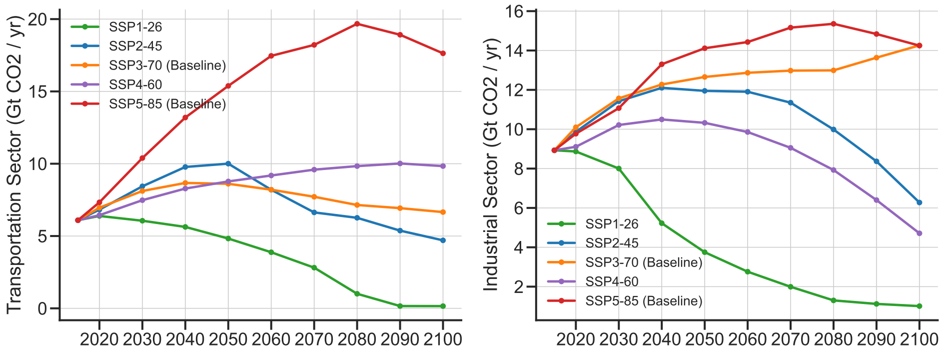


**Fig. 4** $\texttt{CO}_2$ emissions in some of the CIMP6 Scenarios for the transportation (left figure) and industrial (right figure) sectors. See the AR6 Scenario Explorer and Database at https://data.ene.iiasa.ac.at/ar6/.

***Total GHG emissions.***

Using the previous notations, the total GHG emissions is

$$\sum_{\mathsf{e}\in\mathscr{E}^i} \gamma^i_{\mathsf{e},t} = \mathbf{1}\cdot\gamma^i_{\bullet,t}$$

where $\mathbf{1}$ is a vector with unit components in the appropriate dimension equal to $|\mathscr{E}^i|$.

Let $\widetilde{\gamma}^i = (\widetilde{\gamma}^i_t,\, t \geq 0)$ be a carbon emission benchmark (e.g., an SSP of a certain sector to which the $i^{\text{th}}$ obligor belongs to), which is supposed to be a deterministic and measurable function with respect to time. See Figure 4 for such emission benchmarks. At time $t$, the obligor is:

- penalized if its global emission is above $\widetilde{\gamma}^i_t$ through $\ell^i_1\left(\mathbf{1}\cdot\gamma^i_{\bullet,t} - \widetilde{\gamma}^i_t\right)$ where $\ell^i_1$ is a non-decreasing continuous function,
- rewarded if its global emission is below $\widetilde{\gamma}^i_t$ through $\ell^i_2\left(\widetilde{\gamma}^i_t - \mathbf{1}\cdot\gamma^i_{\bullet,t}\right)$ where $\ell^i_2$ is another non-decreasing continuous function.

We further assume that $\ell^i_1, \ell^i_2$ have at most a quadratic growth at infinity. They correspond to national or international policies aimed at incentivizing the reduction of GHG emissions through the establishment of specific quantitative targets. The selection of penalty and reward functions remains a challenging issue for regulatory authorities. Imposing higher penalties, such as exponential penalty functions, may prompt immediate responses from companies. However, this could yield long-term adverse effects on their productivity or competitiveness. Therefore, a well-designed penalty and reward mechanism is crucial for encouraging companies to enhance their adaptation and mitigation measures while maintaining alignment with their business strategies.

**Example 1.** *The functions $\ell^i$ can be taken as*

$$\ell^i_1(x) = \omega^i_1\ x^2_+, \qquad \ell^i_2(x) = \omega^i_2\ x^2_+,$$

*where $x_+ = \max(x, 0)$, and $\omega_1^i, \omega_2^i \geq 0$ are constant parameters representing respectively the penalty and reward forces. We choose a quadratic penalty (resp., reward) function to accentuate large values of over-emission (resp., under-emission) compared to the benchmark emission scenario. This example is further investigated in Theorems 3 and 4. This results in a convex problem that allows for an explicit solution for each obligor and can be solved numerically with fast algorithms for all obligors in the portfolio.*

**Example 2.** *The functions $\ell^i$ can be taken as*

$$\ell_1^i(x) = \omega_1^i \ x_+^2, \qquad \ell_2^i(x) = \omega_2^i \ x_+.$$

*Here, the reward function has a linear growth rate. Compared to the previous example, there is less incentive to pollute less though the cost of polluting remains the same.*

***Production dynamics and profit function.***

We consider the special model where the profit function is given by

$$\pi^i(x) = \mathrm{AP}^i \times \log(x),$$

where $\mathrm{AP}^i$ is a given average price.

To define the stochastic model for the production, consider a filtered probability space $(\Omega, \mathcal{F}, \mathbb{F} = (\mathcal{F}_t)_{t\geq 0}, \mathbb{P})$ on which is defined $n+1$ independent standard Brownian motions $B, B^1, \ldots, B^n$. Given the logarithmic nature of the profit function, we directly model the log-production $p_t^i = \log(P_t^i)$ as a linear stochastic differential equation

$$\begin{aligned} \mathrm{d}p_t^i &= \mu^i(t, p_t^i, \gamma_{\bullet,t}^i)\,\mathrm{d}t + \sigma^i\,\mathrm{d}W_t^i, \\ \mu^i(t, p, \gamma_{\bullet,t}^i) &= a^i - b^i p + \sum_{\mathsf{e}\in\mathscr{E}^i} c_{\mathsf{e}}^i \times \gamma_{\mathsf{e},t}^i \times \theta_{\mathsf{e},t}^i \\ &= a^i - b^i p + c_{\bullet}^{i,\theta} \cdot \gamma_{\bullet,t}^i, \end{aligned} \tag{4}$$

where we have introduced

$$c_{\bullet}^{i,\theta} := (c_{\mathsf{e}}^i \times \theta_{\mathsf{e},t}^i)_{\mathsf{e}\in\mathscr{E}^i}$$

and

$$\mathrm{d}W_t^i = \rho^i\,\mathrm{d}B_t + \sqrt{1-(\rho^i)^2}\,\mathrm{d}B_t^i \tag{5}$$

with correlations $\rho^i \in (-1, 1)$. $B$ reads as a systemic risk factor and the $(B^i)_{1\leq i\leq n}$ as independent idiosyncratic risk factors. We further assume that $\sigma^i > 0$.

In (4), the coefficient $a^i \geq 0$ represents an average production level, $b^i \geq 0$ is a mean-reverting parameter and $c_{\mathsf{e}}^i$ measures the obligor's energy consumption dependence on $\mathsf{e}$. Making $c_{\mathsf{e}}^i$ depend on $\mathsf{e}$ serves as a means to convey that, from the perspective of the $i$th obligor, it is possible to interchange energy sources, even though the power consumption $\gamma_{\mathsf{e}}^i \times \theta_{\mathsf{e}}^i$ remains the same. To illustrate this concept, consider the straightforward example of hydroelectric power generation and fuel usage for vehicle transportation.

### 2.3 The obligor's optimization plan

Each obligor aims to optimize its emission level under the double objectives of maximizing its production profit and respecting the emission mitigation scenario. Mathematically, it corresponds to

$$\widehat{\gamma}^i_\bullet := \arg\sup_{\gamma^i_\bullet \in \mathcal{A}^i} \mathcal{J}^i\left(\gamma^i_\bullet\right), \tag{6}$$

$$\begin{aligned}\mathcal{J}^i\left(\gamma^i_\bullet\right) := \mathbb{E}\Bigg[\int_0^\infty e^{-rt}\Big(&\mathrm{AP}^i\, p^i_t - \alpha^{i,\theta}_{\bullet,t}\cdot\gamma^i_{\bullet,t} - \beta^{i,\theta}_{\bullet,t}\cdot(\gamma^2)^i_{\bullet,t} \\ &- \ell^i_1\left(\mathbf{1}\cdot\gamma^i_{\bullet,t} - \widetilde{\gamma}^i_t\right) + \ell^i_2\left(\widetilde{\gamma}^i_t - \mathbf{1}\cdot\gamma^i_{\bullet,t}\right)\Big)\,\mathrm{d}t\Bigg],\end{aligned} \tag{7}$$

where $r > 0$ is a constant positive discount rate. The admissible stochastic control set $\mathcal{A}^i$ contains all progressively measurable processes $\gamma^i_\bullet$ valued in

$$\prod_{t\geq 0}\mathcal{G}^i_{\bullet,t} \quad \text{with} \quad \mathcal{G}^i_{\bullet,t} = \prod_{\mathsf{e}\in\mathscr{E}^i}[0, \lambda^{\max}_{\mathsf{e},t}] \tag{8}$$

where the function $t \mapsto \lambda^{\max}_{\mathsf{e},t}$ is measurable.

Mathematically, what is important is that the set $\mathcal{G}^i_{\bullet,t}$ is a closed, bounded, and non-empty subset [5] of $[0,+\infty)^{|\mathscr{E}^i|}$.

We assume that the following integrability condition holds: there exists $\eta \in (0, r)$ such that

$$\int_0^\infty e^{-\eta t} \sup_{\gamma^i_{\bullet,t}\in\mathcal{G}^i_{\bullet,t}} |\gamma^i_{\bullet,t}|^2\,\mathrm{d}t < +\infty. \tag{9}$$

In view of (8), the condition writes $\int_0^\infty e^{-\eta t}\sup_{\mathsf{e}\in\mathscr{E}^i}(\lambda^{\max}_{\mathsf{e},t})^2\,\mathrm{d}t < +\infty$.

### 2.4 Existence and uniqueness of an optimal emission

We now characterize the solution $\widehat{\gamma}^i_\bullet$ to the optimization problem (6).

**Theorem 1.** *Let $i \in \{1,\cdots,n\}$ and for any $\gamma_{\bullet,t}$, define*

$$\begin{aligned}f^i_t(\gamma^i_{\bullet,t}) := \frac{\mathrm{AP}^i}{r+b^i}\, c^{i,\theta}_\bullet\cdot\gamma^i_{\bullet,t} - \alpha^{i,\theta}_{\bullet,t}\cdot\gamma^i_{\bullet,t} - \beta^{i,\theta}_{\bullet,t}\cdot(\gamma^2)^i_{\bullet,t} - \\ \ell^i_1\big(\mathbf{1}\cdot\gamma^i_{\bullet,t} - \widetilde{\gamma}^i_t\big) + \ell^i_2\big(\widetilde{\gamma}^i_t - \mathbf{1}\cdot\gamma^i_{\bullet,t}\big).\end{aligned} \tag{10}$$

*Assume that*

[5] Allowing for unbounded $\mathcal{G}^i_t$ is presumably possible but would lead to extra technicalities that are not central to our work. Furthermore, on the application side, restricting to bounded emissions is natural.

- *the benchmark global emission $t \mapsto \widetilde{\gamma}^i_t$ is such that*

$$\int_0^\infty e^{-\eta t} |\widetilde{\gamma}^i_t|^2 \mathrm{d}t < +\infty, \tag{11}$$

- *there exists a $\widehat{\gamma}^i_{\bullet,t} \in \mathcal{G}^i_{\bullet,t}$ maximizing $f^i_t(\cdot)$.*

*Then, this maximizer solves the optimal stochastic control problem (6).*

**Theorem 2.** *Assume that (11) holds, that $\gamma^i_{\bullet,t} \mapsto f^i_t(\gamma^i_{\bullet,t})$ is continuous and strictly concave. Then, there exists a unique $\widehat{\gamma}^i_{\bullet,t} \in \mathcal{G}^i_{\bullet,t}$ maximizing $f^i_t(\cdot)$ and thus solving the optimization problem (6).*

The main advantage of the setting of Theorem 2 compared to that of Theorem 1 is algorithmic, because, in the above *concave case*, we can make use of fast algorithms to compute the maximizer of $f^i_t(\cdot)$, (see, e.g., the projected gradient descent algorithm exposed in Remark 3).

**Theorem 3.** *Consider the loss functions of Example 1, i.e., $\ell^i_1(x) = \omega^i_1(x_+)^2$ and $\ell^i_2(x) = \omega^i_2(x_+)^2$. Then, when $\omega^i_2\big(\mathbf{1} \cdot \frac{1}{\beta^{i,\theta}_{\bullet,t}}\big) < 1$ for any $t \geq 0$, the assumptions of Theorem 2 are satisfied.*

Note that the loss functions of Example 2 do not allow to retrieve a concave problem: as the reader can easily check, this is mainly due to the fact that $g(z) : z \mapsto z^2 - cz_+$ (with $c > 0$) is not a convex function (indeed, $g(\epsilon) + g(-\epsilon) < 2g(0)$ for a small enough $\epsilon > 0$). Despite this lack of convexity, the conditions of Theorem 1 apply: indeed, the function $\gamma^i_{\bullet,t} \mapsto f^i_t(\gamma^i_{\bullet,t})$ is continuous on a compact set $\mathcal{G}^i_t$ and, thus, admits a maximizer. However, the uniqueness is not guaranteed.

*Proof of Theorem 1.* To alleviate notation, we omit the index $i$. Let $\gamma_\bullet = (\gamma_{\mathsf{e}})_{\mathsf{e} \in \mathscr{E}} \in \mathcal{A}$ be an admissible strategy to the problem (7). Then, the difference $J(\widehat{\gamma}_\bullet) - J(\gamma_\bullet)$ equals

$$\begin{aligned} \mathbb{E}\Big[\int_0^\infty e^{-rt}\Big(&\mathrm{AP}\big(\widehat{p}_t - p_t\big) - \alpha^\theta_{\bullet,t} \cdot \big(\widehat{\gamma}_{\bullet,t} - \gamma_{\bullet,t}\big) - \beta^\theta_{\bullet,t} \cdot \big((\widehat{\gamma}^2)_{\bullet,t} - (\gamma^2)_{\bullet,t}\big) \\ &- \ell_1(\mathbf{1} \cdot \widehat{\gamma}_{\bullet,t} - \widetilde{\gamma}_t) + \ell_1(\mathbf{1} \cdot \gamma_{\bullet,t} - \widetilde{\gamma}_t) + \ell_2(\widetilde{\gamma}_t - \mathbf{1} \cdot \widehat{\gamma}_{\bullet,t}) - \ell_2(\widetilde{\gamma}_t - \mathbf{1} \cdot \gamma_{\bullet,t})\Big)\mathrm{d}t\Big] \end{aligned} \tag{12}$$

where $\widehat{p}_t$ is given by

$$\mathrm{d}\widehat{p}_t = (a - b\widehat{p}_t + c^\theta_\bullet \cdot \widehat{\gamma}_{\bullet,t})\mathrm{d}t + \sigma \mathrm{d}W_t, \qquad \widehat{p}_0 = p_0. \tag{13}$$

By Ito's formula, we have

$$\mathrm{d}\big(e^{-rt}(\widehat{p}_t - p_t)\big) = e^{-rt}\Big(-(b+r)(\widehat{p}_t - p_t) + c^\theta_\bullet \cdot (\widehat{\gamma}_{\bullet,t} - \gamma_{\bullet,t})\Big)\mathrm{d}t. \tag{14}$$

Since $\gamma_\bullet \in \mathcal{A}$, we have

$$\mathbb{E}\left[\Big(\int_0^\infty e^{-\eta t}|c^\theta_\bullet \cdot \gamma_{\bullet,t}|\mathrm{d}t\Big)^2\right] \leq \Big(\int_0^\infty (e^{-\eta t/2})^2 \mathrm{d}t\Big)\, \mathbb{E}\left[\int_0^\infty (e^{-\eta t/2}|c^\theta_\bullet \cdot \gamma_{\bullet,t}|)^2 \mathrm{d}t\right]$$

$$\leq \frac{|c^\theta_\bullet|^2}{\eta}\mathbb{E}\left[\int_0^\infty e^{-\eta t}|\gamma_{\bullet,t}|^2 \mathrm{d}t\right] < +\infty$$

using the integrability condition (9). Therefore, the integral $\int_0^\infty e^{-\eta t}|c^\theta_\bullet \cdot \gamma_{\bullet,t}|\mathrm{d}t$ is finite almost surely; the same holds obviously for $\widehat{\gamma}_\bullet$. By solving the equation (13), we get

$$\widehat{p}_t - p_t = \int_0^t e^{-b(t-s)} c^\theta_\bullet \cdot (\widehat{\gamma}_{\bullet,s} - \gamma_{\bullet,s})\mathrm{d}s,$$

$$|e^{-rt}(\widehat{p}_t - p_t)| \leq e^{(\eta-r)t}\int_0^t e^{-\eta s}|c^\theta_\bullet \cdot (\widehat{\gamma}_{\bullet,s} - \gamma_{\bullet,s})|\mathrm{d}s$$

using $b \geq 0$. Hence, since $r > \eta$,

$$\lim_{t\to+\infty} e^{-rt}(\widehat{p}_t - p_t) = 0, \quad \text{a.s.},$$

which leads to

$$\int_0^\infty e^{-rt}\Big(-(b+r)(\widehat{p}_t - p_t) + c^\theta_\bullet \cdot (\widehat{\gamma}_{\bullet,t} - \gamma_{\bullet,t})\Big)\mathrm{d}t = 0, \quad \text{a.s.},$$

owing to (14). Consequently, (12) rewrites as

$$\begin{aligned}
&J(\widehat{\gamma}_\bullet) - J(\gamma_\bullet)\\
&= \mathbb{E}\Bigg[\int_0^\infty e^{-rt}\Bigg(\frac{\mathrm{AP}}{r+b}c^\theta_\bullet \cdot (\widehat{\gamma}_{\bullet,t} - \gamma_{\bullet,t}) - \alpha^\theta_{\bullet,t}\cdot(\widehat{\gamma}_{\bullet,t} - \gamma_{\bullet,t}) - \beta^\theta_{\bullet,t}\cdot\big((\widehat{\gamma}^2)_{\bullet,t} - (\gamma^2)_{\bullet,t}\big)\\
&\qquad - \ell_1(\mathbf{1}\cdot\widehat{\gamma}_{\bullet,t} - \widetilde{\gamma}_t) + \ell_1(\mathbf{1}\cdot\gamma_{\bullet,t} - \widetilde{\gamma}_t) + \ell_2(\widetilde{\gamma}_t - \mathbf{1}\cdot\widehat{\gamma}_{\bullet,t}) - \ell_2(\widetilde{\gamma}_t - \mathbf{1}\cdot\gamma_{\bullet,t})\Bigg)\mathrm{d}t\Bigg]\\
&= \mathbb{E}\left[\int_0^\infty e^{-rt}\Big(f_t(\widehat{\gamma}_{\bullet,t}) - f_t(\gamma_{\bullet,t})\Big)\mathrm{d}t\right].
\end{aligned}$$

As $\widehat{\gamma}_{\bullet,t}$ maximizes $f_t(\cdot)$ for any $t$, we have proved the announced statement. Moreover, we can show that $t \mapsto \widehat{\gamma}_{\bullet,t}$ is measurable, see Appendix B for detail. □

*Proof of Theorem 2.* The strict concavity of $f^i_t(\cdot)$ on the convex set $\mathcal{G}^i_t$ ensures that the set of maximizers of $\widehat{\gamma}^i_{\bullet,t}$ is reduced to a singleton. □

*Proof of Theorem 3.* We omit the index $i$. In view of Theorem 2, it is enough to prove that for any $t$, the continuous function $f_t$ is strictly concave with the current choice of loss functions $\ell_1 = \omega_1(x_+)^2$ and $\ell_2 = \omega_2(x_+)^2$. At any given $t$, the Hessian matrix is

$$\big(D^2 f_t(\gamma_\bullet)\big)_{\mathsf{e},\mathsf{e}'} := \frac{\partial^2 f_t(\gamma_\bullet)}{\partial\gamma_\mathsf{e}\,\partial\gamma_{\mathsf{e}'}} = -2\mathbf{1}_{\mathsf{e}=\mathsf{e}'}\beta^\theta_{\mathsf{e},t} - 2\omega_1\mathbf{1}_{E_t} + 2\omega_2\mathbf{1}_{E^c_t}, \qquad \mathsf{e},\mathsf{e}' \in \mathscr{E},$$

where $E_t := \{\widetilde{\gamma}_t < \mathbf{1}\cdot\gamma_\bullet\}$. On the set of $\gamma_\bullet$ such that $E_t$ holds, then $D^2 f_t(\gamma_\bullet)$ is obviously negative definite because we have assumed $\beta^\theta_{\mathsf{e},t} > 0$ for any $\mathsf{e}$ and $t$, and $\omega_1 \geq$

0. On the complementary set where $\mathbf{1}_{E_t} = 0$, the sign analysis is less straightforward. Let us compute the associated quadratic form: for any non-zero $x_\bullet = (x_\mathsf{e})_{\mathsf{e}\in\mathscr{E}} \in \mathbb{R}^{|\mathscr{E}|}$, we have

$$\begin{aligned}\frac{1}{2} x_\bullet \cdot D^2 f_t(\gamma_\bullet) x_\bullet &= -\sum_{\mathsf{e}\in\mathscr{E}} \beta^\theta_{\mathsf{e},t} x_\mathsf{e}^2 + \omega_2 \big(\sum_{\mathsf{e}\in\mathscr{E}} x_\mathsf{e}\big)^2 \\ &\le -\sum_{\mathsf{e}\in\mathscr{E}} \beta^\theta_{\mathsf{e},t} x_\mathsf{e}^2 + \omega_2 \big(\sum_{\mathsf{e}\in\mathscr{E}} \frac{1}{\beta^\theta_{\mathsf{e},t}}\big)\big(\sum_{\mathsf{e}\in\mathscr{E}} \beta^\theta_{\mathsf{e},t} x_\mathsf{e}^2\big) < 0,\end{aligned}$$

since $\omega_2\big(\sum_{\mathsf{e}\in\mathscr{E}} \frac{1}{\beta^\theta_{\mathsf{e},t}}\big) < 1$ and $\sum_{\mathsf{e}\in\mathscr{E}} \beta^\theta_{\mathsf{e},t} x_\mathsf{e}^2 > 0$. We have proved that, in any case, $D^2 f_t(\gamma_\bullet)$ is negative definite, i.e., $f_t$ is strictly concave. □

## 2.5 An explicit example

We now offer efficient emission strategies with explicit formulas based on Example 1 and Theorem 3.

**Theorem 4.** *Assume that the assumptions of Theorem 3 are in force. For any $t \ge 0$, define*

$$\Gamma^i_t := \frac{\mathbf{1}}{2\beta^{i,\theta}_{\bullet,t}} \cdot \big(\frac{\mathrm{AP}^i\, c^{i,\theta}_\bullet}{r+b^i} - \alpha^{i,\theta}_{\bullet,t}\big), \qquad \xi^i_{1,t} := \omega^i_1 \Big(\mathbf{1} \cdot \frac{1}{\beta^{i,\theta}_{\bullet,t}}\Big), \qquad \xi^i_{2,t} := \omega^i_2 \Big(\mathbf{1} \cdot \frac{1}{\beta^{i,\theta}_{\bullet,t}}\Big)$$

*and assume that for all $\mathsf{e} \in \mathscr{E}^i$,*

$$0 < \frac{\mathrm{AP}^i\, c^{i,\theta}_\mathsf{e}}{r+b^i} - \alpha^{i,\theta}_{\mathsf{e},t} - \frac{2\omega^i_1}{1+\xi^i_{1,t}}\big(\Gamma^i_t - \widetilde{\gamma}^i_t\big)^+ - \frac{2\omega^i_2}{1-\xi^i_{2,t}}\big(\widetilde{\gamma}^i_t - \Gamma^i_t\big)^+ < 2\beta^{i,\theta}_{\mathsf{e},t} \lambda^{\max}_{\mathsf{e},t}. \tag{15}$$

*Then, the optimal emission strategy for the energy source $\mathsf{e}$ has the explicit form*

$$\widehat{\gamma}^i_{\mathsf{e},t} = \frac{1}{2\beta^{i,\theta}_{\mathsf{e},t}} \Big(\frac{\mathrm{AP}^i\, c^{i,\theta}_\mathsf{e}}{r+b^i} - \alpha^{i,\theta}_{\mathsf{e},t} - \frac{2\omega^i_1}{1+\xi^i_{1,t}}\,\big(\Gamma^i_t - \widetilde{\gamma}^i_t\big)^+ - \frac{2\omega^i_2}{1-\xi^i_{2,t}}\,\big(\widetilde{\gamma}^i_t - \Gamma^i_t\big)^+\Big). \tag{16}$$

*Furthermore, the excess emission equals*

$$\mathbf{1} \cdot \widehat{\gamma}^i_{\bullet,t} - \widetilde{\gamma}^i_t = \frac{1}{1+\xi^i_{1,t}}\big(\Gamma^i_t - \widetilde{\gamma}^i_t\big)^+ - \frac{1}{1-\xi^i_{2,t}}\big(\widetilde{\gamma}^i_t - \Gamma^i_t\big)^+. \tag{17}$$

*Proof.* We compute the gradient of (10). For any $t \ge 0$ and energy source $\mathsf{e} \in \mathscr{E}^i$,

$$\frac{\partial f^i_t}{\partial \gamma^i_{\mathsf{e},t}}(\gamma^i_{\bullet,t}) = \frac{\mathrm{AP}^i\, c^{i,\theta}_\mathsf{e}}{r+b^i} - \alpha^{i,\theta}_{\mathsf{e},t} - 2\beta^{i,\theta}_{\mathsf{e},t}\gamma^i_{\mathsf{e},t} - 2\omega^i_1\big(\mathbf{1}\cdot\gamma^i_{\bullet,t} - \widetilde{\gamma}^i_t\big)_+ - 2\omega^i_2\big(\widetilde{\gamma}^i_t - \mathbf{1}\cdot\gamma^i_{\bullet,t}\big)_+. \tag{18}$$

From Theorem 3, we know that $f^i_t$ is strictly concave so that it is enough to check that $\widehat{\gamma}^i_{\mathsf{e},t}$ given by (16) is in $\big(0, \lambda^{\max}_{\mathsf{e},t}\big)$ (the interior of the constraint set) and cancels (18). The verification that $\widehat{\gamma}^i_{\mathsf{e},t} \in \big(0, \lambda^{\max}_{\mathsf{e},t}\big)$ is immediate from the condition (15).

Let us now verify that $\widehat{\gamma}^i_{\mathtt{e},t}$ cancels (18) and verifies (17). Consider the first case where $\Gamma^i_t \geq \widetilde{\gamma}^i_t$: summing over $\mathtt{e}$ in (16), we have

$$\begin{aligned}\mathbf{1}\cdot\widehat{\gamma}^i_{\bullet,t} - \widetilde{\gamma}^i_t &= \Gamma^i_t - \frac{\xi^i_{1,t}}{1+\xi^i_{1,t}}\big(\Gamma^i_t - \widetilde{\gamma}^i_t\big) - \widetilde{\gamma}^i_t \\ &= \frac{1}{1+\xi^i_{1,t}}\big(\Gamma^i_t - \widetilde{\gamma}^i_t\big),\end{aligned}$$

and therefore, we get

$$\begin{aligned}\frac{\partial f^i_t}{\partial \gamma^i_{\mathtt{e},t}}(\widehat{\gamma}^i_{\bullet,t}) &= \frac{\mathrm{AP}^i\, c^{i,\theta}_{\mathtt{e}}}{r+b^i} - \alpha^{i,\theta}_{\mathtt{e},t} - \left(\frac{\mathrm{AP}^i\, c^{i,\theta}_{\mathtt{e}}}{r+b^i} - \alpha^{i,\theta}_{\mathtt{e},t} - \frac{2\omega^i_1}{1+\xi^i_{1,t}}\big(\Gamma^i_t - \widetilde{\gamma}^i_t\big)\right) - \frac{2\omega^i_1}{1+\xi^i_{1,t}}\big(\Gamma^i_t - \widetilde{\gamma}^i_t\big) \\ &= 0.\end{aligned}$$

Consider now the second case where $\Gamma^i_t < \widetilde{\gamma}^i_t$. A similar computation gives

$$\begin{aligned}\widetilde{\gamma}^i_t - \mathbf{1}\cdot\widehat{\gamma}^i_{\bullet,t} &= \widetilde{\gamma}^i_t - \Gamma^i_t + \frac{\xi^i_{2,t}}{1-\xi^i_{2,t}}\big(\widetilde{\gamma}^i_t - \Gamma^i_t\big) \\ &= \frac{1}{1-\xi^i_{2,t}}\big(\widetilde{\gamma}^i_t - \Gamma^i_t\big)\end{aligned}$$

and consequently, it readily follows that

$$\begin{aligned}\frac{\partial f^i_t}{\partial \gamma^i_{\mathtt{e},t}}(\widehat{\gamma}^i_{\bullet,t}) &= \frac{\mathrm{AP}^i\, c^{i,\theta}_{\mathtt{e}}}{r+b^i} - \alpha^{i,\theta}_{\mathtt{e},t} - \left(\frac{\mathrm{AP}^i\, c^{i,\theta}_{\mathtt{e}}}{r+b^i} - \alpha^{i,\theta}_{\mathtt{e},t} - \frac{2\omega^i_2}{1-\xi^i_{2,t}}\big(\widetilde{\gamma}^i_t - \Gamma^i_t\big)\right) - \frac{2\omega^i_2}{1-\xi^i_{2,t}}\big(\widetilde{\gamma}^i_t - \Gamma^i_t\big) \\ &= 0.\end{aligned}$$

The proof is complete. $\square$

**Remark 1.** *The interpretations of the above results are as follows. First, when there is no penalty or reward policy, then the obligor's optimal emission strategy for each energy* $\mathtt{e}$ *is*

$$\frac{1}{2\beta^{i,\theta}_{\mathtt{e},t}}\left(\frac{c^{i,\theta}_{\mathtt{e}}}{r+b^i} - \alpha^{i,\theta}_{\mathtt{e},t}\right).$$

*When the incentive policies are incorporated, that is, when* $\omega_1$ *and* $\omega_2$ *become strictly positive, the obligor reduces its emissions level. Second, the price of a given energy* $\alpha^{i,\theta}_{\mathtt{e},t}$ *is bounded from above by a certain level so that the energy* $\mathtt{e}$ *is chosen by the obligor. In the opposite case, the emission by the corresponding energy may drop to zero, meaning that the obligor prefers to avoid* $\mathtt{e}$ *and choose other types of energy.*

We conclude this section by illustrating, in Figure 5, the outputs of Theorem 4. Namely, we consider the scenario SSP1-26 for the industrial sector and three energy types (natural gas, electricity from nuclear, and electricity from coal). We use the values of Table 2 for the power/$\mathtt{CO_2e}$ ratios and Figure 2 for the prices. More precisely, the parameters are $r = 0.05$, $a = b = 0$, $c = (1,1,1)$, $\omega_1 = 10^{-4}$, $\omega_2 = 0$, $\alpha = (0.05, 0.16, 0.16)$, $\beta = (1,1,1)$, $\theta = (1/0.202, 1/0.012, 1/0.820)/3600$. As expected in view of the SSP1-26 scenario (right plot of Figure 4), the total emission gets reduced as time goes by, and the reduction mainly impacts the browner sources of energy (first coal, second natural gas).

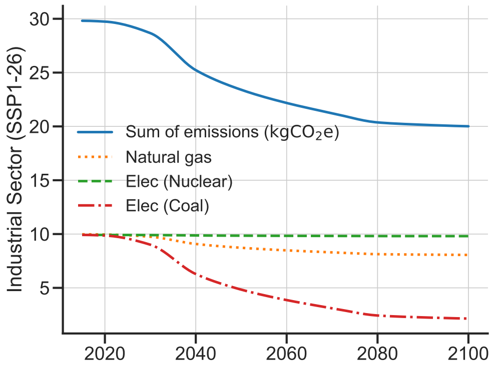


**Fig. 5** Optimal emissions for three types of energy: natural gas, electricity from nuclear, and electricity from coal. Scenario: SSP1-26. Sector: Industrial.

# 3 Modeling the physical risk of each portfolio obligor

Now, we model the physical risk and its effect on the obligor's value process. Inspired by actuarial science, especially ruin theory [1], we model our aggregate loss as a compound Poisson process, capturing the randomness of physical risk events in time, independent inter-arrival intervals, and random losses denoted as $Z$. Our goal, however, is to provide a more tailored analysis specific to the obligor of interest. In our study, we incorporate the temporal evolution of the magnitude of physical risks, offering a detailed and dynamic perspective on how these risks affect the obligor.

## 3.1 Disintegrating the physical risk over climate and weather event types

In our modeling, we aim to consider two specific aspects:

1. Not all climate and weather events are relevant to a particular obligor.
2. The obligor's exposures vary based on the geographical zones of its offices and factories.

Climate extremes (droughts, heatwaves, sea level rise, etc) pertain to long-term, persistent deviations from typical climate conditions, while weather extreme events (tornadoes, blizzards, tsunamis, etc) are short-term, intense deviations from normal weather patterns. They both occur on different timescales (typically from hours to a few days for weather-extreme events) and have distinct characteristics. Types of climate extremes and weather extreme events `cw` are extensively detailed in [39] and consist of

$$
\begin{aligned}
\mathcal{CW} := \big\{ & \text{storm/typhoon/hurricane/tornado/tropical cyclone,} \\
& \text{hailstorm, flood, winter storm, level sea rise, and storm surge,} \\
& \text{heat wave, drought, wildfire, extreme cold spells, snowstorms, and blizzards,} \ldots \big\}.
\end{aligned}
$$

For each climate and weather event $\mathtt{cw}$ and geographical zone $l$, we associate a Poisson process $N^{\mathtt{cw},l}$ (defined on the same filtered probability space as before) with a deterministic intensity $t \mapsto \lambda_t^{\mathtt{cw},l}$. The intensity varies over time due to the global impact of climate change, which increases the frequency of extreme weather events. However, the outcome is location-dependent, with some areas experiencing heightened frequencies while others may see decreases. We refer to [21] for the mathematical definition of a time-inhomogeneous Poisson process. While these Poisson processes could be defined with interdependencies, they do not affect the subsequent derivation, as we demonstrate.

When a climate and weather event $\mathtt{cw}$ occurs in a geographical zone $l$ and time $u$, the $i$th obligor experiences an immediate loss $Z_u^{i,\mathtt{cw},l}$ [6] resulting from the obligor's vulnerability and exposure to climate events. Over a time interval $[t_0, t_1]$, the cumulative loss incurred by the $i$th obligor is

$$\int_{t_0}^{t_1} \sum_{\mathtt{cw},l} Z_u^{i,\mathtt{cw},l} \, \mathrm{d}N_u^{\mathtt{cw},l}.$$

## 3.2 Expected loss for an obligor

The obligor is making provisions for these physical risks by discounting future losses with an interest rate $r$. This leads to the following definition of the Expected Physical Loss (EPL) as follows:

$$\mathrm{EPL}^i(t) := \mathbb{E}\Big[ \sum_{\mathtt{cw},l} \int_t^{\infty} e^{-r(u-t)} Z_u^{i,\mathtt{cw},l} \mathrm{d}N_u^{\mathtt{cw},l} \big| \mathcal{F}_t \Big]. \tag{19}$$

From the properties of the compound process, we have

$$\mathrm{EPL}^i(t) = \int_t^{\infty} e^{-r(u-t)} \Big( \sum_{\mathtt{cw},l} \mathbb{E}\big[Z_u^{i,\mathtt{cw},l}\big] \, \lambda_u^{\mathtt{cw},l} \Big) \mathrm{d}u, \tag{20}$$

where we have additionally assumed that the random losses $(Z_u^{i,\mathtt{cw},l})_u$ are independent (in time) – this is a standard assumption in actuarial sciences.

Alternatively to the above Expected Physical Loss, we could better capture the full distribution of the physical losses, i.e. the term $\sum_{\mathtt{cw},l} \int \cdots$ in (19), by computing quantile-based measures (e.g., Value-at-Risk). This approach is commonly used in the

[6] on the mathematical side, $Z^{i,\mathtt{cw},l}$ is a càglàd process

Solvency II framework with the Minimum Capital Requirement (MCR) and Solvency Capital Requirement (SCR). This option is briefly discussed in Remark 1.

### 3.3 Calibration procedure

To use the above description, we have to model the time evolution of

$$u \mapsto \mathbb{E}\big[Z_u^{i,\texttt{cw},l}\big], \qquad u \mapsto \lambda_u^{\texttt{cw},l},$$

according to each geographical zone $l$ and climate and weather event $\texttt{cw}$.

Empirical studies, like [19], reveal a strong connection between the frequencies $\lambda_u^{\texttt{cw},l}$ of climate events, mean losses $\mathbb{E}\big[Z_u^{i,\texttt{cw},l}\big]$, and the climate mitigation trajectory linked to a specific SSP. In a scenario like SSP5, characterized by significant warming, obligors would face more frequent and substantial losses. Conversely, in a greener, highly mitigated scenario such as SSP1, losses would be far less frequent and severe. We suggest a simplified, realistic model suitable for straightforward calibration.

From the Nordhaus model [30, 31] (also known as the DICE model – Dynamic Integrated model of Climate and the Economy), we know that $\mathbb{E}\big[Z_u^{i,\texttt{cw},l}\big]$ and $\lambda_u^{\texttt{cw},l}$ depend on the global rise in atmospheric temperature $\mathcal{T}_{\text{ATM}}$ through a damage function $\mathcal{D}$. In the initial DICE model, the damage is quadratic:

$$\mathcal{D}\big(\mathcal{T}_{\text{ATM}}\big) = a_1 \mathcal{T}_{\text{ATM}} + a_2 \mathcal{T}_{\text{ATM}}^2 \tag{21}$$

with $a_1 = 0$, $a_2 = 0.0028388$ (2008 version of DICE). Alternative functions have been proposed in the literature; see [17, 41], for instance. Note that $\mathcal{T}_{\text{ATM}}$ refers to the global average temperature increase relative to the pre-industrial era. For simplicity, we assume the damage function is identical for all companies and independent of $\texttt{cw}$ and $l$.

We assume that $\sum_{\texttt{cw},l} \mathbb{E}\big[Z_u^{i,\texttt{cw},l}\big]\, \lambda_u^{\texttt{cw},l}$ evolves proportionally to $\mathcal{D}(\mathcal{T}_{\text{ATM}}(u))$, where the path of the atmosphere temperature is given by the selected SSP and denoted $u \to \mathcal{T}_{\text{ATM}}(u)$, see Figure 6 for some relative temperature paths for different SSP scenarios. All in all, our model of physical losses for the $i$th obligor becomes

$$\text{EPL}^i(t) := \Big(\sum_{\texttt{cw},l} \mathbb{E}\big[Z_{t_{\text{ref}}}^{i,\texttt{cw},l}\big] \lambda_{t_{\text{ref}}}^{\texttt{cw},l}\Big) \int_t^\infty e^{-r(u-t)} \frac{\mathcal{D}(\mathcal{T}_{\text{ATM}}(u))}{\mathcal{D}(\mathcal{T}_{\text{ATM}}(t_{\text{ref}}))} \mathrm{d}u, \tag{22}$$

where $t_{\text{ref}}$ is the time at which the model is calibrated.

Calculating the total physical losses of the obligor $\Big(\sum_{\texttt{cw},l} \mathbb{E}\big[Z_{t_{\text{ref}}}^{i,\texttt{cw},l}\big] \lambda_{t_{\text{ref}}}^{\texttt{cw},l}\Big)$ is based on historical obligor data. Note that we are not accounting for any changes the obligor may have made to its operations or locations in recent years. Observe also that the integral factor is common across all companies. In essence, when evaluating future physical risk, we begin with historical losses and apply a scenario-dependent multiplicative factor

$$\int_t^\infty e^{-r(u-t)} \frac{\mathcal{D}(\mathcal{T}_{\text{ATM}}(u))}{\mathcal{D}(\mathcal{T}_{\text{ATM}}(t_{\text{ref}}))} \mathrm{d}u.$$

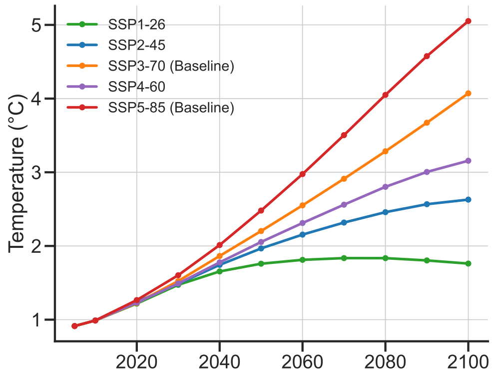


**Fig. 6** Global average temperature increase relative to the pre-industrial era (year 1750) for different SSPs. Source: [35], https://ourworldindata.org/.

**Remark 1.** *To more effectively capture the full distribution of physical losses, we could define a Value-at-Risk-based measure at risk level $\alpha$, thereby replacing $\mathrm{EPL}^i$ in (19) with*

$$\mathrm{VaR}_\alpha\text{-}\mathrm{PL}^i(t) = \int_t^\infty e^{-r(u-t)}\,\mathrm{VaR}_\alpha\Big[\sum_{\mathtt{cw},l}\int_{u-1}^u Z_s^{i,\mathtt{cw},l}\,\mathrm{d}N_s^{\mathtt{cw},l}\,\mathrm{d}s\Big]\,\mathrm{d}u. \tag{23}$$

*The quantity $\mathrm{PL}_u^i := \sum_{\mathtt{cw},l}\int_{u-1}^u Z_s^{i,\mathtt{cw},l}\,\mathrm{d}N_s^{\mathtt{cw},l}\,\mathrm{d}s$ represents the physical loss incurred by the ith obligor over a one-year period ending at time $u$. By applying similar arguments to those used for the estimation of $\mathrm{EPL}^i$, the $\mathrm{VaR}_\alpha\text{-}\mathrm{PL}^i$ metrics can be derived via DICE-rescaling as*

$$\widehat{\mathrm{VaR}_\alpha\text{-}\mathrm{PL}}^i(t) = \mathrm{VaR}_\alpha\big[\mathrm{PL}^i_{t_{ref}}\big]\int_t^\infty e^{-r(u-t)}\,\frac{\mathcal{D}(\mathcal{T}_{\mathrm{ATM}}(u))}{\mathcal{D}(\mathcal{T}_{\mathrm{ATM}}(t_{ref}))}\,\mathrm{d}u. \tag{24}$$

*Additionally, the quantity $\mathrm{VaR}_\alpha\big[\mathrm{PL}^i_{t_{ref}}\big]$ can be inferred from historical physical loss data.*

# 4 Obligor's default probability in an explicit model

We model the default event as in the structural credit approach, [37, Chapter 3]. At a given time $t \geq 0$, an obligor defaults if its value is inferior to its debt and liability level. The probability of default for the $i$th obligor is

$$\mathrm{PD}_t^i = \mathbb{P}\left(\widehat{V}_t^i \leq L^i(t)\right)$$

where the obligor's value $\widehat{V}_t^i$ is impacted by both transition and physical risks, and the default barrier $L^i(t)$ is a deterministic function which represents the minimal level of the obligor's liability payment such as the debt reimbursement and the labor cost of the obligor at time $t$.

In the following, we define the obligor's value $\widehat{V}_t^i$ as the conditional discounted value of the obligor's future cashflow at time $t \geq 0$ with the optimal emission strategy $\widehat{\gamma}^i$, minus the expected physical losses (19). We also take losses functions $\ell_1(\cdot), \ell_2(\cdot)$ to be the same as in Example 1. This yields

$$\begin{aligned}\widehat{V}_t^i := \mathbb{E}\Bigg[\int_t^\infty e^{-r(u-t)}\Big(&\mathrm{AP}^i \times \widehat{P}_u^i - \alpha_{\bullet,u}^{i,\theta} \cdot \widehat{\gamma}_{\bullet,u}^i - \beta_{\bullet,u}^{i,\theta} \cdot (\widehat{\gamma}^2)_{\bullet,u}^i \\ &- \omega_1^i \left(\mathbf{1} \cdot \widehat{\gamma}_{\bullet,u}^i - \widetilde{\gamma}_u^i\right)_+^2 + \omega_2^i \left(\widetilde{\gamma}_u^i - \mathbf{1} \cdot \widehat{\gamma}_{\bullet,u}^i\right)_+^2\Big)\mathrm{d}u\Bigg|\mathcal{F}_t\Bigg] \\ &- \mathrm{EPL}^i(t),\end{aligned} \tag{25}$$

where $\widehat{P}^i$ denotes the optimal production associated with $\widehat{\gamma}_\bullet^i$. We note that although the optimization is conducted with the logarithmic function, we here use the total production for the computation of the obligor's value.

Recall that in the explicit model of Section 2.5, the optimal emission $\widehat{\gamma}_\bullet^i$ is deterministic and explicitly given by (16). When the benchmark $\widetilde{\gamma}^i$ is low (strict mitigation scenario), the penalty coefficient $\omega_1^i$ plays an essential role in the optimal strategy, while for a relatively loose scenario when the benchmark is high, the reward coefficient $\omega_2^i$ is more important.

To facilitate the subsequent aggregation of losses across different obligors, let us first describe the stochastic distribution of log production. From (4) and (5), the optimal log production $\widehat{p}^i$ is

$$\begin{aligned}\widehat{p}_u^i = e^{-b^i(u-t)}\widehat{p}_t^i + \frac{a^i}{b^i}(1 - e^{-b^i(u-t)}) + \int_t^u e^{-b^i(u-s)}(c_\bullet^{i,\theta} \cdot \widehat{\gamma}_{\bullet,s}^i)\mathrm{d}s \\ + \sigma^i \int_t^u e^{-b^i(u-s)}\left(\rho^i \mathrm{d}B_s + \sqrt{1-(\rho^i)^2}\,\mathrm{d}B_s^i\right),\end{aligned} \tag{26}$$

for all $u \geq t$.

Conditionally on $\mathcal{F}_t$, $\left(\widehat{p}_u^i\right)_{1\leq i\leq n}$ is an $n$-dimensional Gaussian vector with conditional mean

$$\begin{aligned}\mathbb{E}\left[\widehat{p}_u^i|\mathcal{F}_t\right] &= e^{-b^i(u-t)}\widehat{p}_t^i + \frac{a^i}{b^i}(1 - e^{-b^i(u-t)}) + \int_t^u e^{-b^i(u-s)}(c_\bullet^{i,\theta} \cdot \widehat{\gamma}_{\bullet,s}^i)\,\mathrm{d}s \\ &=: e^{-b^i(u-t)}\widehat{p}_t^i + m^i(u,t),\end{aligned} \tag{27}$$

and conditional covariance

$$\mathrm{Cov}\left(\widehat{p}_u^i, \widehat{p}_u^j|\mathcal{F}_t\right) := \Sigma^{i,j}(u-t) = \sigma^i\sigma^j\left(\rho^i\rho^j\mathbf{1}_{i\neq j} + \mathbf{1}_{i=j}\right)\frac{1 - e^{-(b^i+b^j)(u-t)}}{b^i + b^j}, \tag{28}$$

for every $i, j \in \{1, \ldots, n\}$.

# 5 Aggregated loss distribution of the portfolio

## 5.1 Modeling the loss

In this section, we consider the loss portfolio and its computation. Let the loss portfolio be defined as

$$\mathcal{L}_t = \sum_{i=1}^{n} \Lambda^i \times \mathbf{1}_{\left\{\widehat{V}_t^i \leq L^i(t)\right\}} \tag{29}$$

where $\Lambda^i = \mathrm{EAD}^i \times \mathrm{LGD}^i$ and $\mathrm{LGD}^i, \mathrm{EAD}^i$ are respectively the loss given default and exposure at default associated with the $i$th obligor. The time horizon $t$ is typically chosen to be one year according to the solvency regulation. If interested in longer-time horizons, conditional losses can also be considered as our problem setting is Markovian.

From (22), (25), and the fact that $\mathbb{E}\big[\widehat{P}_u^i|\mathcal{F}_t\big] = \exp\big(e^{-b^i(u-t)}\widehat{p}_t^i + m^i(u,t) + \frac{1}{2}\Sigma^{i,i}(u-t)\big)$, we have

$$\widehat{V}_t^i = h^i\big(t, \widehat{p}_t^i\big)$$

where the deterministic function $h^i(\cdot,\cdot)$ is defined for all $t \geq 0$ and $x \in \mathbb{R}$ as

$$\begin{aligned} h^i(t,x) &:= \mathrm{AP}^i \int_t^\infty e^{-r(u-t)} \exp\Big(e^{-b^i(u-t)}x + m^i(u,t) + \frac{1}{2}\Sigma^{i,i}(u-t)\Big)\,\mathrm{d}u \\ &- \int_t^\infty e^{-r(u-t)} \Big(\alpha^{i,\theta}_{\bullet,u} \cdot \widehat{\gamma}^i_{\bullet,u} + \beta^{i,\theta}_{\bullet,u} \cdot (\widehat{\gamma}^2)^i_{\bullet,u} + \omega_1^i\big(\mathbf{1} \cdot \widehat{\gamma}^i_{\bullet,u} - \widetilde{\gamma}^i_u\big)_+^2 - \omega_2^i\big(\widetilde{\gamma}^i_u - \mathbf{1} \cdot \widehat{\gamma}^i_{\bullet,u}\big)_+^2\Big)\,\mathrm{d}u \\ &- \mathrm{EPL}^i(t). \end{aligned} \tag{30}$$

Note that $h^i(t,\cdot)$ is a continuous increasing bijection from $\mathbb{R}$ to $(0,+\infty)$, for any $t$.

The portfolio loss rewrites as

$$\begin{aligned} \mathcal{L}_t &= \sum_{i=1}^{n} \Lambda^i\,\mathbf{1}_{\left\{h^i(t,\widehat{p}_t^i) \leq L^i(t)\right\}} \\ &= \sum_{i=1}^{n} \Lambda^i\,\mathbf{1}_{\left\{\widehat{p}_t^i \leq (h^i(t,\cdot))^{-1}(L^i(t))\right\}} \\ &= \sum_{i=1}^{n} \Lambda^i\,\mathbf{1}_{\left\{e^{-b^i t}\,\widehat{p}_0^i + m^i(t,0) + \sigma^i\sqrt{1-(\rho^i)^2}\int_0^t e^{-b^i(t-s)}\,\mathrm{d}B_s^i - (h^i(t,\cdot))^{-1}(L^i(t)) \leq -\sigma^i\rho^i\int_0^t e^{-b^i(t-s)}\,\mathrm{d}B_s\right\}} \\ &= \sum_{i=1}^{n} \Lambda^i\,\mathbf{1}_{\left\{A_t^i \leq X_t^i\right\}} \end{aligned}$$

with
$$\begin{aligned} A_t^i &:= \frac{1}{\sigma^i}\left[e^{-b^i t}\,\widehat{p}_0^i + m^i(t,0) + \sigma^i\sqrt{1-(\rho^i)^2}\int_0^t e^{-b^i(t-s)}\,\mathrm{d}B_s^i - (h^i(t,\cdot))^{-1}(L^i(t))\right], \\ X_t^i &:= -\rho^i \int_0^t e^{-b^i(t-s)}\,\mathrm{d}B_s. \end{aligned}$$

Analyzing the distribution of $\mathcal{L}_t$ is intricate. Analytical methods are not suitable due to it being a weighted sum of correlated Bernoulli random variables with varying dependencies. An alternative Monte Carlo simulation is feasible but time-consuming for several reasons: a) in typical cases, there are many obligors ($n$ is large); b) the number of correlated Gaussian random variables is large (as large as $n$) making sampling $\mathcal{L}_t$ costly; c) numerous $\mathcal{L}_t$ samples are required, especially for tail event risk management.

To tackle these challenges, we utilize two efficient dimension reduction methods, leveraging multiple enhancements.

- The distribution of the vector $X_t = (X_t^i)_{1\leq i\leq n}$ is Gaussian. An initial, naive assumption might be that the rank of its covariance matrix $K_{X_t}$ approximately equals the number of distinct $b^i$, and that all eigenvalues hold significant importance. However, this intuition is considerably flawed. A thorough examination of the spectral decomposition of $K_{X_t}$ reveals a surprising result: the top two eigenvalues account for over 99% of the total variance (i.e., the trace of $K_{X_t}$). Consequently, we first perform a Principal Component Analysis (PCA) on the vector $X_t$, reducing it to two principal factors. For an in-depth analysis, refer to Section 5.2.
- This approach allows us to express the loss $\mathcal{L}_t$ as a sum of indicator functions with $n$ independent Gaussian random variables (for $\int_0^t e^{-b^i(t-s)}\mathrm{d}B_s^i$) and two common factors derived from the PCA. Utilizing a two-dimensional Polynomial Chaos Expansion (PCE) for indicator functions as outlined in [6], and retaining the first $M$ terms (typically $M = 6$ or 10 suffices), we further approximate $\mathcal{L}_t$ using a multivariate Gaussian random variable with a dimension of $M + 2$ and involving a summation of $M^2$ terms, instead of $2n$ Gaussian random variables and $n$ terms in the sum. Recall that typically $n \approx 10^6$ for major banks: in comparison with the new cost $M^2 \lessapprox 100$, the improvement in complexity is huge. This is elaborated in Subsection 5.3.

In summary, this significantly reduces the overall computational cost of our climate credit model.

## 5.2 Principal Component Analysis (PCA) of $X_t := (X_t^i)_{1\leq i\leq n}$

Let $K_{X_t} = \left((K_{X_t})^{i,j}\right)_{1\leq i,j\leq n}$ be the covariance matrix of $X_t$. We have

$$(K_{X_t})^{i,j} := \mathrm{Cov}(X_t^i, X_t^j) = \rho^i\rho^j \int_0^t e^{-b^i(t-s)}e^{-b^j(t-s)}\mathrm{d}s = \rho^i\rho^j\frac{1-e^{-(b^i+b^j)t}}{b^i+b^j}. \quad (31)$$

Following [11, Section 3.2], the spectral decomposition of $K_{X_t}$ writes as

$$K_{X_t} = \sum_{k=1}^{n} \nu^k u^k (u^k)^\top$$

where $(\nu^k)_{1\leq k\leq n}$ are the eigenvalues (in decreasing order) and $(u^k)_{1\leq k\leq n}$ are the eigenvectors of $K_{X_t}$. Since the latter is a positive semi-definite matrix, $\nu^k \geq 0$ for all

$k$. Equivalently,

$$X_t = \sum_{k=1}^{n} \sqrt{\nu^k} G^k u^k \tag{32}$$

where the $(G^k)_{1 \le k \le n}$ are independent $\mathcal{N}(0,1)$ random variables.

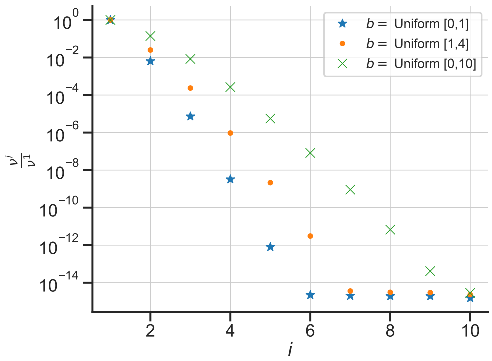


**Fig. 7** Ratio $\frac{\nu^k}{\nu^1}$ for $k$ from 1 to 10 with $n = 1000$, $\rho \sim \mathcal{U}[-1,1]$ and $b \sim \mathcal{U}[0,1], \mathcal{U}[1,4]$, and $\mathcal{U}[0,10]$.

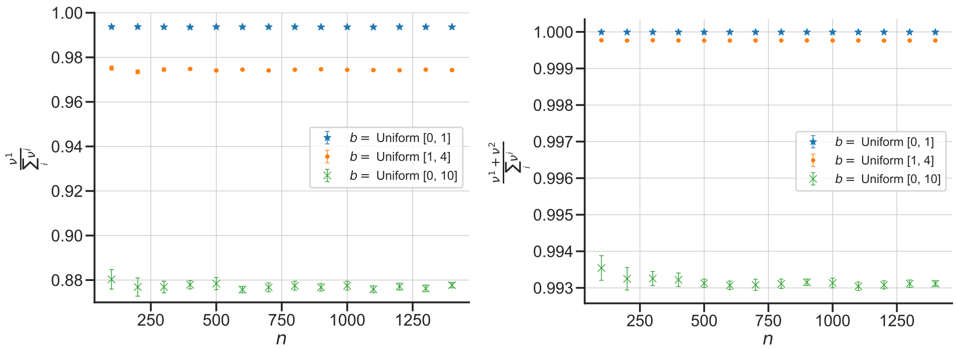


**Fig. 8** Ratio $\frac{\nu^1}{\sum_{k=1}^n \nu^k}$ (left) and $\frac{\nu^1+\nu^2}{\sum_{k=1}^n \nu^k}$ (right) for $n$ from 100 to 1500, $\rho \sim \mathcal{U}[-1,1]$ and $b \sim \mathcal{U}[0,1]$, $\mathcal{U}[1,4]$, and $\mathcal{U}[0,10]$. For each ratio, we provide the 95% confidence interval with 30 independent runs.

Note that when the $b^i$ are constant (say equal to $b > 0$), we can write $K_{X_t} = \boldsymbol{\rho}\boldsymbol{\rho}^\top \frac{1-e^{-2bt}}{2b}$ (where $\boldsymbol{\rho}$ is the vector of $\rho^i$) and therefore, the rank of $K_{X_t}$ equals 1 at most ($\nu^k = 0$ for $k = 2, \cdots n$). For non-constant $b$, we observe (see Figures 7 and 8) that $K_{X_t}$ generally resembles a low-rank symmetric matrix, where only the first two eigenvalues $\nu^1$ and $\nu^2$ matter. This can be assessed using the inertia:

$$\frac{\sum_{k=1}^2 \nu^k}{\sum_{k=1}^n \nu^k}.$$

The above depends on $b^i$ and $n$ and in our experiments, it is very close to 1. namely, we take $\rho^i \sim \mathcal{U}[-1,1]$ and three distinct cases for the $b^i$:

- $b^i \sim \mathcal{U}[0,1]$: the rank of $K_{X_t}$ is very close to one, corresponding to the scenario where $b$ is nearly constant.
- $b^i \sim \mathcal{U}[1,4]$: this is the typical case in practice, the characteristic time $1/b$ falls between one quarter and one year.
- $b^i \sim \mathcal{U}[0,10]$: to illustrate that a rank-two approximation remains acceptable even as the variance increases.

In Figure 7, we plot the ratio $\nu^k/\nu^1$ from $k = 1$ to 10 with $n = 1000$ for a single realization of $\rho^i$ and $b^i$. The plot demonstrates that the ratio decreases extremely rapidly. Specifically, when $b^i \sim \mathcal{U}[0,10]$, the ratio $\nu^3/\nu^1 \approx 10^{-2}$, and it is close to $10^{-5}$ when $b^i \sim \mathcal{U}[0,1]$. In Figure 8, we plot $\frac{\nu^1}{\sum_k \nu^k}, \frac{\nu^1+\nu^2}{\sum_k \nu^k}$, using boxplots over 100 replications for $n$ ranging from 100 to 1500. The results show that the two eigenvalues account for 99% of the total variance when $b^i \sim \mathcal{U}[0,10]$, and 99.99% otherwise. We have not yet been able to precisely quantify this property theoretically, including the selection of the reduced dimension. Furthermore, to the best of our knowledge, this phenomenon has not been documented in the existing literature on random matrices.

We now leverage these experimental observations to approximate the distribution of $X_t$ with a low-dimensional Gaussian distribution. We choose to truncate (32) and keep only 2 terms:

$$X_t \approx \sum_{k=1}^{2} \sqrt{\nu^k} G^k u^k. \tag{33}$$

Denoting the coordinates of the two eigenvectors $u^1, u^2$ by $u^{1,i}, u^{2,i}$ for $i = 1, \dots, n$, the above expansion leads to an approximate model

$$\mathcal{L}_t \approx \mathcal{L}_t^{\mathrm{PCA}} := \sum_{i=1}^{n} \Lambda^i \, \mathbf{1}_{\left\{A_t^i \leq \sqrt{\nu^1} G^1 u^{1,i} + \sqrt{\nu^2} G^2 u^{2,i}\right\}}. \tag{34}$$

**Proposition 5.** *The $L_1$ error between the original and approximated loss is bounded as follows:*

$$\mathbb{E}\left[\left|\mathcal{L}_t - \mathcal{L}_t^{\mathrm{PCA}}\right|\right] \leq \sum_{i=1}^{n} \frac{\Lambda^i}{\pi} \frac{|\rho^i|}{\sqrt{1-(\rho^i)^2}} \sqrt{\frac{\sum_{k=3}^{n} \nu^k (u^{k,i})^2}{\sum_{k=1}^{n} \nu^k (u^{k,i})^2}}. \tag{35}$$

The smaller the eigenvalues ($\nu^k, k \geq 3$) compared to the others, the better the approximation. We have focused on the PCA approximation, but we do not claim that the dependence of constants is optimal with respect to the probabilistic characteristics of $A_t^i$. In particular, the estimate (35) does not account for the fact that we compute tail risks (the indicator functions in (29) are likely equal to 0, which is not reflected on the right-hand side of (35)).

*Proof.* A direct triangular inequality yields

$$\mathbb{E}\left[\left|\mathcal{L}_t - \mathcal{L}_t^{\mathrm{PCA}}\right|\right] \le \sum_{i=1}^{n} \Lambda^i \, \mathbb{E}\left[\left|\mathbf{1}_{\left\{A_t^i \le X_t^i\right\}} - \mathbf{1}_{\left\{A_t^i \le \sqrt{\nu^1} G^1 u^{1,i} + \sqrt{\nu^2} G^2 u^{2,i}\right\}}\right|\right]. \tag{36}$$

To bound the above, we use bounds on the distribution of $A_t^i$. Recall that $A_t^i$ has a Gaussian distribution with variance $(1-(\rho^i)^2)\frac{1-e^{-2b^i t}}{2b^i}$. Observe that we have the identity

$$(\rho^i)^2 \frac{1-e^{-2b^i t}}{2b^i} = \sum_{k=1}^{n} \nu^k (u^{k,i})^2;$$

this follows from the comparison of (31) and (32). Hence, the Gaussian density of $A_t^i$ is uniformly bounded by

$$\frac{1}{\sqrt{2\pi}\sqrt{\sum_{k\ge 1} \nu^k (u^{k,i})^2}} \frac{|\rho^i|}{\sqrt{1-(\rho^i)^2}}.$$

If $X_t^i > \sqrt{\nu^1} G^1 u^{1,i} + \sqrt{\nu^2} G^2 u^{2,i}$, the difference of indicator functions in the right-hand side of (36) equals $\mathbf{1}_{\left\{\sqrt{\nu^1} G^1 u^{1,i} + \sqrt{\nu^2} G^2 u^{2,i} < A_t^i \le X_t^i\right\}}$; in the other case, it is equal to $-\mathbf{1}_{\left\{X_t^i < A_t^i \le \sqrt{\nu^1} G^1 u^{1,i} + \sqrt{\nu^2} G^2 u^{2,i}\right\}}$. Since $A_t^i$ is independent of $X_t^i$ and $\sqrt{\nu^1} G^1 u^{1,i} + \sqrt{\nu^2} G^2 u^{2,i}$, we get

$$\begin{aligned}
&\mathbb{E}\left[\left|\mathbf{1}_{\left\{A_t^i \le X_t^i\right\}} - \mathbf{1}_{\left\{A_t^i \le \sqrt{\nu^1} G^1 u^{1,i} + \sqrt{\nu^2} G^2 u^{2,i}\right\}}\right|\right] \\
&\qquad \le \frac{1}{\sqrt{2\pi}\sqrt{\sum_{k=1}^{n} \nu^k (u^{k,i})^2}} \frac{|\rho^i|}{\sqrt{1-(\rho^i)^2}} \mathbb{E}\left[\left|X_t^i - \sqrt{\nu^1} G^1 u^{1,i} + \sqrt{\nu^2} G^2 u^{2,i}\right|\right]
\end{aligned}$$

The quantity inside in the absolute value is Gaussian distributed with mean zero and variance

$$\sum_{k=3}^{n} \nu^k (u^{k,i})^2.$$

In addition, we have $\mathbb{E}\left[|G^1|\right] = \sqrt{\frac{2}{\pi}}$. All in all, we obtain

$$\mathbb{E}\left[\left|\mathbf{1}_{\left\{A_t^i \le X_t^i\right\}} - \mathbf{1}_{\left\{A_t^i \le \sqrt{\nu^1} G^1 u^{1,i} + \sqrt{\nu^2} G^2 u^{2,i}\right\}}\right|\right] \le \frac{1}{\pi} \frac{|\rho^i|}{\sqrt{1-(\rho^i)^2}} \sqrt{\frac{\sum_{k=3}^{n} \nu^k (u^{k,i})^2}{\sum_{k=1}^{n} \nu^k (u^{k,i})^2}}.$$

Plugging this into (36) readily completes the proof. $\square$

### 5.3 Polynomial chaos expansion (PCE)

We further approximate $\mathcal{L}^{\mathrm{PCA}}$ using a polynomial chaos expansion (PCE). Write

$$\begin{aligned}\mathcal{L}_t^{\mathrm{PCA}} &= \sum_{i=1}^n \Lambda^i \,\mathbf{1}_{\left\{\frac{A_t^i}{\sqrt{\nu^1(u^{1,i})^2+\nu^2(u^{2,i})^2}} \le \frac{\sqrt{\nu^1}u^{1,i}G^1+\sqrt{\nu^2}u^{2,i}G^2}{\sqrt{\nu^1(u^{1,i})^2+\nu^2(u^{2,i})^2}}\right\}} \\ &=: \sum_{i=1}^n \Lambda^i \,\mathbf{1}_{\left\{\tilde{A}_t^i \le L^{1,i}G^1+L^{2,i}G^2\right\}}\end{aligned}$$

with $L^{k,i} := \frac{\sqrt{\nu^k}u^{k,i}}{\sqrt{\nu^1(u^{1,i})^2+\nu^2(u^{2,i})^2}}$ for $k=1,2$ so that $(L^{1,i})^2+(L^{2,i})^2=1$ and $\tilde{A}_t^i := \frac{A_t^i}{\sqrt{\nu^1(u^{1,i})^2+\nu^2(u^{2,i})^2}}$. Observing that $L^{1,i}G^1+L^{2,i}G^2 \sim \mathcal{N}(0,1)$, we apply a PCE of the indicator function at order $M$ (see Proposition 6) to get

$$\begin{aligned}\mathcal{L}_t^{\mathrm{PCA,PCE}} &:= \sum_{i=1}^n \Lambda^i \sum_{m=0}^M \tau_m(\tilde{A}_t^i)\,\mathrm{He}_m(L^{1,i}G^1+L^{2,i}G^2) \\ &= \sum_{i=1}^n \Lambda^i \sum_{m=0}^M \tau_m(\tilde{A}_t^i) \sum_{\substack{m_1,m_2\ge 0\\ m_1+m_2=m}} \frac{m!}{m_1!m_2!}(L^{1,i})^{m_1}(L^{2,i})^{m_2}\mathrm{He}_{m_1}(G^1)\mathrm{He}_{m_2}(G^2)\end{aligned}$$

where we have used [6, Lemma 3.5] at the second equality. Introducing the new random variables

$$\varepsilon_{n,m_1,m_2} := \sum_{i=1}^n \Lambda^i\,\tau_{m_1+m_2}(\tilde{A}_t^i)\frac{(m_1+m_2)!}{m_1!m_2!}(L^{1,i})^{m_1}(L^{2,i})^{m_2},$$

the approximate portfolio loss rewrites as

$$\mathcal{L}_t^{\mathrm{PCA,PCE}} = \sum_{m=0}^M \sum_{\substack{m_1,m_2\ge 0\\ m_1+m_2=m}} \varepsilon_{n,m_1,m_2}\mathrm{He}_{m_1}(G^1)\mathrm{He}_{m_2}(G^2). \tag{37}$$

In the approximation of large $n$, the $\varepsilon_{n,m_1,m_2}$ being sums of independent random variables, we can approximate the $\frac{1}{2}(M+2)(M+1)$-dimensional vector $\left(\varepsilon_{n,m_1,m_2}\right)_{m_1+m_2=m,\,0\le m\le M}$ with a Gaussian vector $(\varepsilon^{\mathrm{G}}_{n,m_1,m_2})$ with mean vector $\mathcal{M}$

and covariance matrix $\mathcal{K}$ where for every $0 \le m_1, m_1', m_2, m_2' \le M$, we have

$$
\begin{aligned}
\mathcal{M}_{m_1,m_2} &:= \mathbb{E}\left[\varepsilon_{n,m_1,m_2}\right] = \sum_{i=1}^{n} \Lambda^i \, \mathbb{E}\left[\tau_{m_1+m_2}\left(\tilde{A}_t^i\right)\right] \frac{(m_1+m_2)!}{m_1!\, m_2!} (L^{1,i})^{m_1} (L^{2,i})^{m_2}, \\
\mathcal{K}_{(m_1,m_2),(m_1',m_2')} &:= \operatorname{Cov}\left(\varepsilon_{n,m_1,m_2}, \varepsilon_{n,m_1',m_2'}\right) \\
&= \sum_{i=1}^{n} (\Lambda^i)^2 \operatorname{Cov}\left(\tau_{m_1+m_2}\left(\tilde{A}_t^i\right), \tau_{m_1'+m_2'}\left(\tilde{A}_t^i\right)\right) \\
&\qquad \times \frac{(m_1+m_2)!}{m_1!\, m_2!} (L^{1,i})^{m_1} (L^{2,i})^{m_2} \frac{(m_1'+m_2')!}{m_1'!\, m_2'!} (L^{1,i})^{m_1'} (L^{2,i})^{m_2'},
\end{aligned}
\tag{38}
$$

taking advantage of the independence of $(\tilde{A}_t^i)_{1 \le i \le n}$. Our PCA-PCE portfolio loss with Gaussian approximation finally writes as

$$
\mathcal{L}_t^{\mathrm{PCA,PCE,G}} := \sum_{m=0}^{M} \sum_{\substack{m_1,m_2 \ge 0 \\ m_1+m_2=m}} \varepsilon_{n,m_1,m_2}^{\mathrm{G}} \mathrm{He}_{m_1}(G^1) \mathrm{He}_{m_2}(G^2).
$$

The parameters $\mathcal{M}, \mathcal{K}$ can be efficiently computed either thanks to recursive relations, see Proposition 7 for details, or via simple Gauss–Hermite quadratures. The $L_2$ error due to the truncation between $\mathcal{L}^{\mathrm{PCA}}$ and $\mathcal{L}^{\mathrm{PCA,PCE}}$ is of order $(\sum_{i=1}^{n} \Lambda^i) M^{-\frac{1}{4}}$. Refined estimates for the $L_2$ error are provided in [7, Theorem 2.7].

## 5.4 Numerical experiments

In this section, we aim to evaluate our methodology, focusing specifically on two key aspects: the improvement in computational speed and the performance of the PCA-PCE-based approximation. Additionally, we seek to assess the impact of physical risk on the portfolio loss.

We focus on three distinct SSP scenarios: SSP1-26, SSP3-70 (Baseline), and SSP5-85 (Baseline) for the transportation sector, see Figure 4. The portfolio loss maturity is set at $t = 5$ years, where $t = 0$ corresponds to 2015. We take $n_{\mathrm{mc}} = 10^5$ Monte Carlo samples for our analysis. We study the fictitious portfolio $\mathcal{A}$ with parameters:

***Portfolio $\mathcal{A}$:***
$t = 5$ years, $n = 1,000$, $r = 2\%$, 3 different energy sources for $\mathtt{e}$, $c_{\mathtt{e}}^i = (0.01, 0.01, 0.01)$, $\omega_1 = 0.05$, $\omega_2 = 0.02$, $\alpha_{\bullet,t}^i = (0,0,0)$, $\beta_{\bullet,t}^i = (0.1, 0.5, 0.8)$, $\theta_{\bullet,t}^i = (1,1,1)$, $P_0 = 1$, $\sigma^i \overset{\text{i.i.d.}}{\sim} \mathcal{U}[0, \frac{1}{2}]$, $a^i \overset{\text{i.i.d.}}{\sim} \mathcal{U}[0, \frac{1}{2}]$, $b^i \overset{\text{i.i.d.}}{\sim} \mathcal{U}[1, 4]$, $\rho^i \overset{\text{i.i.d.}}{\sim} \mathcal{U}[-1, 1]$, $\Lambda^i = \frac{1}{\sqrt{i}}$, $\mathrm{AP}^i = 1$, $\lambda_{\mathrm{ref}} = 3\%$.

### 5.4.1 Physical Risk Impact

In light of Section 3, to account for the physical risk associated with the portfolio, we must compute the expected physical loss $\mathrm{EPL}^i$ for each obligor $i$. From (25), we observe that when accounting for physical risk, the default barrier $L^i(t)$ increases by the amount $\mathrm{EPL}^i$.

To compute $\mathrm{EPL}^i$ as described in (22), we assume that the sum of the total physical losses amounts to 0.001% of the obligor's current value. This is represented by $\sum_{\mathtt{cw},l} \mathbb{E}\big[Z^{i,\mathtt{cw},l}_{t_{\mathrm{ref}}}\big]\lambda^{\mathtt{cw},l}_{t_{\mathrm{ref}}} = 0.001\% \times \widehat{V}^i_0$. The damage function $\mathcal{D}$ is defined in (21).

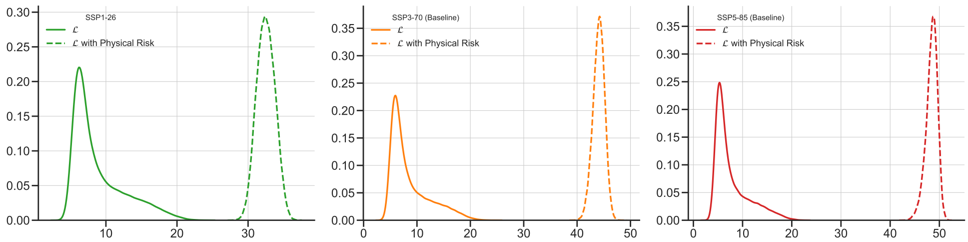


**Fig. 9** Portfolio losses with and without physical risk when $t = 5$ years for the scenarios SSP1-26, SSP3-70, and SSP5-85.

As anticipated, we see in Figure 9 that incorporating a physical risk term significantly shifts the portfolio loss distribution upward. In the subsequent numerical tests assessing the accuracy of PCA-PCE approximations, we eliminate physical risk by setting $\mathrm{EPL}^i(t) = 0$ for all $i$, and focus solely on the transition risk component.

### 5.4.2 PCA approximation

We now evaluate the PCA approximation. In Figure 10, we present the density plots of the loss portfolio and the two-factor-PCA-approximated loss. As anticipated from the analysis in Section 5.2, the PCA approximation is highly accurate, with the two densities appearing virtually identical.

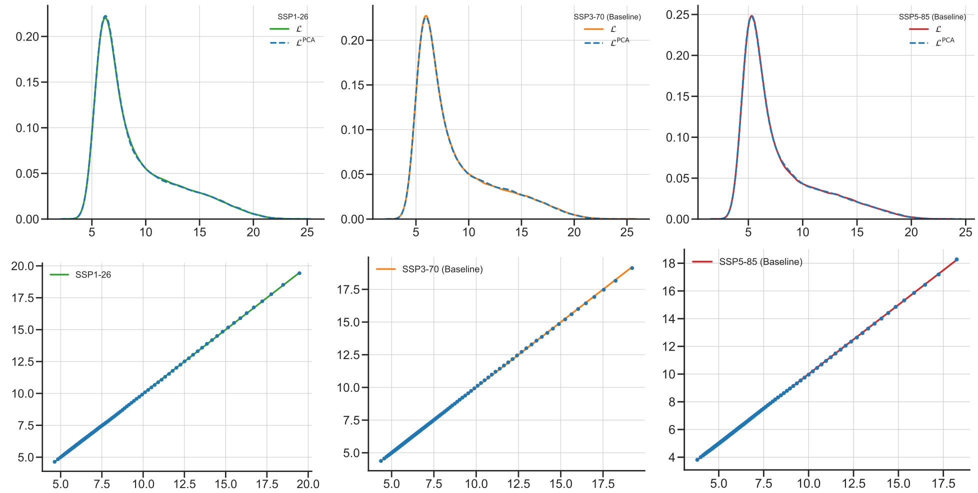


**Fig. 10** Portfolio loss $\mathcal{L}$ and two-factor-PCA-approximated loss $\mathcal{L}^{\mathrm{PCA}}$ when $t = 5$ years for the scenarios SSP1-26, SSP3-70, and SSP5-85 (top figures) and associated Q-Q plots (bottom figures).

### 5.4.3 PCA-PCE approximation

Next, we assess the PCA-PCE-approximated loss for truncation parameters $M \in \{1, 3, 5, 10\}$ along with the respective Q-Q plot, see Figure 11. As expected, the approximation improves with higher values of $M$.

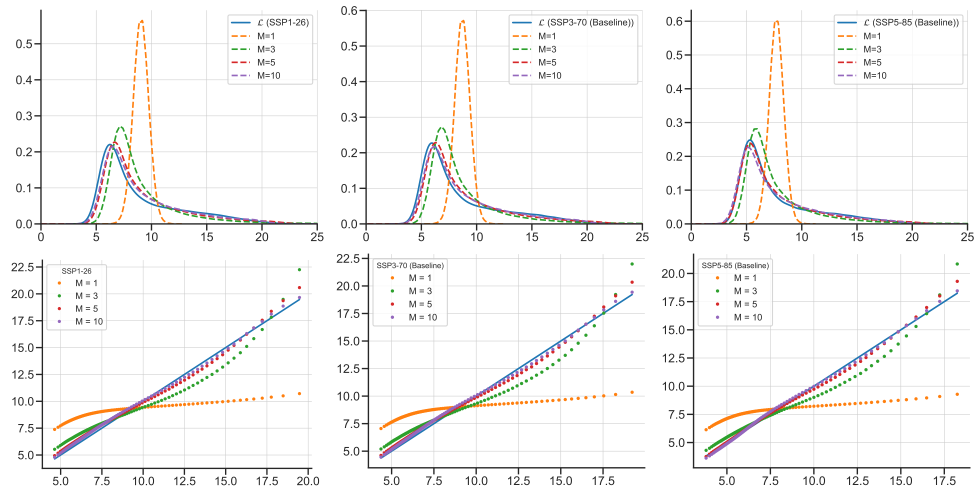


**Fig. 11** Comparison of $\mathcal{L}$ and $\mathcal{L}^{\mathrm{PCA,PCE,G}}$ (left figures) and associated Q-Q plots (right figures) with $M = 1, 3, 5$ and 10 when $t = 5$ years for the scenarios SSP1-26, SSP3-70, and SSP5-85.

Let us further describe the numerical implementations of our PCA-PCE approximation for the portfolio loss $\mathcal{L}$. We assume that all parameters listed in Table 3 are available.

For each scenario, we begin by pre-computing the PCA decomposition of the covariance matrix $K_X$, see (31), along with the mean and covariance of the vector $\varepsilon$ for the PCE. Next, we perform a Monte Carlo simulation to obtain $n_{\text{mc}}$ samples of the approximated loss $\mathcal{L}^{\text{PCA,PCE}}$, as described in Algorithm 2.

As an example, when $n = 10,000$ obligors and $n_{\text{mc}} = 10^5$ Monte Carlo samples, Algorithm 1 takes approximately 75 seconds, while Algorithm 2 takes approximately 2 seconds. For both Algorithms, the pre-computation of $L^i(t)$ and $\widehat{\gamma}_t^i$ takes about 10 minutes.

---

**Algorithm 1:** Crude Monte Carlo: Sampling of the portfolio loss $\mathcal{L}_t$

---

**Output**: $n_{\text{mc}}$ i.i.d. samples of $\mathcal{L}_t$;
**for** $j \leftarrow 1$ **to** $n_{\text{mc}}$ **do**
  Compute vector of optimal emissions $(\widehat{\gamma}_t^1, \dots, \widehat{\gamma}_t^n)$, see Theorem 4;
  Sample Gaussian vector $(\widehat{p}_t^1, \dots, \widehat{p}_t^n)$, see (27) and (28);
  Compute vector of optimal values $(\widehat{V}_t^1, \dots, \widehat{V}_t^n)$ where $\widehat{V}^i(t) = h^i(t, \widehat{p}_t^i)$, see (30);
  Compute the portfolio loss $\mathcal{L}_t = \sum_{i=1}^n \Lambda^i \times \mathbf{1}_{\left\{\widehat{V}_t^i \le L^i(t)\right\}}$, see (29).
**end**

---

**Algorithm 2:** Monte Carlo: Sampling of the PCA-PCE portfolio loss with Gaussian approximation (with loss functions as in Example 1)

---

**Output**: $n_{\text{mc}}$ i.i.d. samples of $\mathcal{L}_t^{\text{PCA,PCE,G}}$;
**Offline computation**:
 Find PCA decomposition of the covariance matrix $K_{X_t}$, see Section 5.2;
Compute parameters $\mathcal{M}, \mathcal{K}$ (38) for the PCE using recursive relations in Proposition 7;
**for** $j \leftarrow 1$ **to** $n_{\text{mc}}$ **do**
  Sample $\left(\varepsilon^{\text{G}}_{n,m_1,m_2}\right)_{m_1+m_2=m,\, 0\le m\le M} \sim \mathcal{N}(\mathcal{M}, \mathcal{K})$;
  Sample two independent $G^1, G^2 \sim \mathcal{N}(0,1)$;
  Compute PCA-PCE portfolio loss with Gaussian approximation $\mathcal{L}_t^{\text{PCA,PCE,G}} = \sum_{m=0}^M \sum_{\substack{m_1,m_2\ge 0\\ m_1+m_2=m}} \varepsilon^{\text{G}}_{n,m_1,m_2} \text{He}_{m_1}(G^1)\text{He}_{m_2}(G^2)$, see (37);
**end**

---

**Remark 2.** *To calibrate the default boundary $L^i(t)$, we proceed as in [5, Section 3.2.]. Given a default intensity rate $\lambda^i_{\text{ref}}$ for the ith obligor, $L^i(t)$ is determined such that*

$$\mathbb{P}\left(\widehat{V}_t^i(\omega_1 = \omega_2 = 0) \le L^i(t)\right) = 1 - e^{-\lambda^i_{\text{ref}}\, t},$$

*where $\widehat{V}_t^i(\omega_1 = \omega_2 = 0)$ corresponds to the optimal obligor's value with no reward or penalization.*

**Remark 3** (Projected gradient descent to compute $\widehat{\gamma}^i_{\bullet,t}$ under the setting of Theorem 2)**.** *In general, there is no closed-form solution for the optimal emissions. To numerically solve*

$$\operatorname*{arg\,max}_{\gamma_\bullet \in \mathcal{G}^i_{\bullet,t}} f^i_t(\gamma_\bullet), \tag{39}$$

*we can use a projected gradient descent (PGD) [8]. More precisely, we first use gradient descent and then perform a projection onto $\mathcal{G}^i_{\bullet,t}$, see (8). At the $k^{th}$ iteration, we set for each energy source $\mathsf{e} \in \mathscr{E}^i$,*

$$\gamma^{i,(k+1)}_{\mathsf{e},t} = \mathrm{Proj}_{[0,\lambda^{\max}_{\mathsf{e},t}]}\left(\gamma^{i,(k)}_{\mathsf{e},t} - \eta_k \frac{\partial}{\partial \gamma^i_{\mathsf{e},t}} f^i_t(\gamma^{i,(k)}_{\mathsf{e},t})\right) = \left(\gamma^{i,(k)}_{\mathsf{e},t} - \eta_k \frac{\partial}{\partial \gamma^i_{\mathsf{e},t}} f^i_t(\gamma^{i,(k)}_{\mathsf{e},t})\right)^+ \wedge \lambda^{\max}_{\mathsf{e},t},$$

*where $\eta_k$ is the step-size.*

*Recall from [29, Section 2.1] that if $g$ is a convex and $L$-smooth function on $\mathbb{R}^d$ then the convergence rate for a gradient descent $\gamma^{(k)} = \gamma^{(k-1)} - \eta_k \nabla g(\gamma^{(k-1)})$ is $g(\gamma^{(k)}) - g(\widehat{\gamma}) \leq \mathcal{O}(1/k)$. If in addition $g$ is $\mu$-strongly convex [7], $g(\gamma^{(k)}) - g(\widehat{\gamma}) \leq \mathcal{O}((1-\mu/L)^k) = \mathcal{O}(e^{-k(\mu/L)})$ where $k$ is the number of iterations. Because the projection is onto a closed convex set, the convergence rates remain the same for (39), see [29, Section 2.2.5].*

*Defining $A := -x_\bullet \cdot D^2 f_t(\gamma_\bullet) x_\bullet$, we observe that:*

$$A = 2\Big(\sum_{\mathsf{e}\in\mathscr{E}} \beta^\theta_{\mathsf{e},t} x^2_{\mathsf{e}} - \omega_2 \big(\sum_{\mathsf{e}\in\mathscr{E}} x_{\mathsf{e}}\big)^2\Big) \geq 2\Big(\sum_{\mathsf{e}\in\mathscr{E}} \beta^\theta_{\mathsf{e},t} x^2_{\mathsf{e}} \Big(1 - \omega_2 \sum_{\mathsf{e}\in\mathscr{E}} \frac{1}{\beta^\theta_{\mathsf{e},t}}\Big)\Big) \geq \mu \sum_{\mathsf{e}\in\mathscr{E}} x^2_{\mathsf{e}},$$

*where $\mu = 2\min_{\mathsf{e}'\in\mathscr{E}^i} \beta^\theta_{\mathsf{e}',t}\Big(1 - \omega_2 \sum_{\mathsf{e}\in\mathscr{E}} \frac{1}{\beta^\theta_{\mathsf{e},t}}\Big)$. Similarly, $A \leq L\sum_{\mathsf{e}\in\mathscr{E}} x^2_{\mathsf{e}}$ with $L = 2\max_{\mathsf{e}\in\mathscr{E}^i} \beta_{\mathsf{e},t}$. Consequently, $-f_t(\cdot)$ is convex, $L$-smooth, and $\mu$-strongly convex, which ensures that a PGD has the exponential convergence rate $\mathcal{O}(e^{-k(\mu/L)})$.*

# 6 Conclusion

We have designed an end-to-end methodology to assess the credit risk of a large portfolio of obligors impacted by transition and physical climate risks, addressing both modeling and computational challenges. Our model takes as input an SSP scenario, transforms it into an optimal emission strategy for each obligor based on its characteristics, and then deduces the impact on the obligor's firm value within a structural credit modeling framework. The aggregation of individual losses across the large portfolio is achieved using two dimension-reduction techniques–Principal Component Analysis and Polynomial Chaos Expansion–proven to be efficient and accurate. In the near future, we will apply the whole procedure to real data.

[7] A differentiable function $f : \mathbb{R}^d \to \mathbb{R}$ is $L$-smooth if $f(y) \leq f(x) + \nabla f(x)\cdot(y-x) + \frac{L}{2}\|y-x\|^2$ and is $\mu$-strongly convex with $\mu > 0$ if $f(y) \geq f(x) + \nabla f(x)\cdot(y-x) + \frac{\mu}{2}\|y-x\|^2$ for all $x, y \in \mathbb{R}^d$.

# A Polynomial Chaos Expansion

For any $m \in \mathbb{N}$, denote $\mathrm{He}_m(x) := (-1)^m e^{\frac{x^2}{2}} \frac{\mathrm{d}^m}{\mathrm{d}x^m}\left(e^{-\frac{x^2}{2}}\right)$ the probabilist's Hermite polynomials. They satisfy the three-term recurrence relation

$$\mathrm{He}_0(x) = 1, \quad \mathrm{He}_1(x) = x, \quad \mathrm{He}_{m+2}(x) = x\mathrm{He}_{m+1}(x) - (m+1)\mathrm{He}_m(x), \qquad \forall m \in \mathbb{N}.$$

For a detailed account of Hermite polynomials, see [32, Chapter 18].

**Proposition 6** ([7, Proposition 2.2 for Hermite polynomials])**.** *Let $c \in \mathbb{R}$ and $Z \in \mathbb{R}$. Then,*

$$\mathbf{1}_{c \le Z} = \sum_{m=0}^{\infty} \tau_m(c)\,\mathrm{He}_m(Z)$$

*where $\tau_0(c) = \Phi(-c)$ and $\tau_m(c) = \frac{e^{-\frac{c^2}{2}}}{m!\sqrt{2\pi}}\mathrm{He}_{m-1}(c)$ for all $m \in \mathbb{N}^*$. The equality holds for all $Z \neq c$.*

**Proposition 7** ([6, Proposition 3.1])**.** *Let $a \in \mathbb{R}^*, b \in \mathbb{R}$ and $X \sim \mathcal{N}(0,1)$. For every $i, j \in \mathbb{N}$, define*

$$\begin{aligned} \mu_i(a,b) &:= \mathbb{E}\left[\tau_i(aX+b)\right], \\ \sigma_{i,j}(a,b) &:= \mathrm{Cov}\left(\tau_i(aX+b), \tau_j(aX+b)\right). \end{aligned}$$

*Then, the following recursive relations hold:*

$$\begin{cases} \mu_0(a,b) = \Phi\left(-\frac{b}{\sqrt{1+a^2}}\right), \qquad \mu_1(a,b) = \frac{e^{-\frac{b^2}{2(1+a^2)}}}{\sqrt{2\pi}\sqrt{1+a^2}}, \\ \mu_{i+2}(a,b) = \frac{b}{(i+2)(1+a^2)}\mu_{i+1}(a,b) - \frac{i}{(i+2)(i+1)(1+a^2)}\mu_i(a,b), \end{cases}$$

$$\begin{cases} \sigma_{0,0}(a,b) = \Phi_\Sigma\left((-b,-b)^\top\right) - \mu_0(a,b)^2, \quad \Sigma = \begin{pmatrix} 1+a^2 & a^2 \\ a^2 & 1+a^2 \end{pmatrix}. \\ \sigma_{0,1}(a,b) = \mu_1(a,b)\left(\mu_0\left(\frac{a}{\sqrt{1+a^2}}, \frac{b}{1+a^2}\right) - \mu_0(a,b)\right), \\ \sigma_{0,i+2}(a,b) = \frac{b}{(i+2)(1+a^2)}\sigma_{0,i+1}(a,b) - \frac{i}{(i+1)(i+2)(1+a^2)}\sigma_{0,i}(a,b) \\ \qquad\qquad - \frac{a^2}{(i+2)(1+a^2)}\mu_1(a,b)\mu_{i+1}\left(\frac{a}{\sqrt{1+a^2}}, \frac{b}{1+a^2}\right), \\ \sigma_{i+1,j+1}(a,b) = \frac{1}{a^2(i+1)}\left[-\left(1+a^2\right)(j+2)\,\sigma_{i,j+2}(a,b) + b\sigma_{i,j+1}(a,b) - \frac{j}{j+1}\sigma_{i,j}(a,b)\right] \\ \qquad\qquad - \mu_{i+1}(a,b)\mu_{j+1}(a,b), \end{cases}$$

*where for all $x \in \mathbb{R}^2$, $\Phi_\Sigma(x) := \mathbb{P}(Y \le x)$ and $Y \sim \mathcal{N}(0, \Sigma)$ with $\Sigma$ positive definite.*

# B Proof of measurability in time for Theorem 1

We show that the (deterministic) optimal solution $\widehat{\gamma}_{\bullet,t}$ of Theorem 1 is measurable in time. Let $d = |\mathscr{E}^i|$. We use the notation $f(t, \boldsymbol{x}) : [0, +\infty) \times \mathbb{R}^d \to \mathbb{R}$ to denote the function $f_t^i(\cdot)$ defined in (10) by

$$f_t^i(\boldsymbol{x}) := \frac{\mathrm{AP}^i}{r+b^i}\, c_\bullet^{i,\theta} \cdot \boldsymbol{x} - \alpha_{\bullet,t}^{i,\theta} \cdot \boldsymbol{x} - \beta_{\bullet,t}^{i,\theta} \cdot \boldsymbol{x}^2 - \ell_1^i \big(\mathbf{1} \cdot \boldsymbol{x} - \widetilde{\gamma}_t^i\big) + \ell_2^i \big(\widetilde{\gamma}_t^i - \mathbf{1} \cdot \boldsymbol{x}\big)$$

where for any $\boldsymbol{x} = (x_1, \cdots, x_d)$, the notation $\boldsymbol{x}^2$ denotes the vector $(x_1^2, \cdots, x_d^2)$. The standing assumptions are

1. For any $\boldsymbol{x} \in \mathbb{R}^d$, $f(\cdot, \boldsymbol{x}) : \mathbb{R}^+ \to \mathbb{R}$ is measurable.
2. For any $t \in \mathbb{R}^+$, $f(t, \cdot) : \mathbb{R}^d \to \mathbb{R}$ is continuous.

For the sake of notational simplicity in (8), we rewrite the set $\mathcal{G}_{\bullet,t}^i$ as

$$\mathcal{G}_t := [0, \lambda_1(t)] \times \cdots \times [0, \lambda_d(t)],$$

for some measurable (in time) mappings $\lambda_i$. This is a compact subset of $\mathbb{R}^d$. We define a new function extending $f(t, \cdot)$ outside $\mathcal{G}_t$ as

$$g : \begin{cases} \mathbb{R}^+ \times \mathbb{R}^d & \to \mathbb{R}, \\ (t, x) & \mapsto f(t, \boldsymbol{x}) \mathbf{1}_{\boldsymbol{x} \in \mathcal{G}_t} - \infty \mathbf{1}_{\boldsymbol{x} \notin \mathcal{G}_t} \end{cases}.$$

Since the $\lambda_i$'s are measurable, the indicator functions are measurable in time (for any given $\boldsymbol{x} \in \mathbb{R}^d$), and since $f(\cdot, \boldsymbol{x})$ is measurable too, $g(\cdot, \boldsymbol{x})$ is measurable in time. Owing to the form of $\mathcal{G}_t$ and the continuity of $f$ in the second variable, observe that

$$\widehat{f}(t) := \max_{\boldsymbol{x} \in \mathcal{G}_t} f(t, \boldsymbol{x}) = \sup_{\boldsymbol{x} \in \mathbb{Q}} g(t, \boldsymbol{x}).$$

As a countable supremum of measurable functions, $\widehat{f}$ is a measurable mapping.

Now, denote by $\boldsymbol{x}_t^* \in \mathcal{G}_t$ the point that maximizes $f(t, \cdot)$ on $\mathcal{G}_t$. Let us show that $\mathcal{T} := \{t \in \mathbb{R}^+ : \boldsymbol{x}_t^* \le \bar{\boldsymbol{x}}\}$ is a measurable set for any given $\bar{\boldsymbol{x}} \in \mathbb{R}^d$. Observe that

$$\mathcal{T} = \bigcap_{m=1}^{\infty} \bigcup_{\boldsymbol{x} \in \mathbb{Q}, \boldsymbol{x} \le \bar{\boldsymbol{x}}} \Big\{ g(t, \boldsymbol{x}) \ge \widehat{f}(t) - \frac{1}{m} \Big\},$$

i.e., $\mathcal{T}$ is a countable intersection of countable unions of measurable sets, thus it is a measurable set. □

# C Model parameters

# References


[1] Asmussen, S. and Albrecher, H. (2010). *Ruin Probabilities.* World Scientific.

[2] Basel Committee on Banking Supervision (2021). Climate-related risk drivers and their transmission channels. *Bank for International Settlements*, d517. https://www.bis.org/bcbs/publ/d517.htm.

| **Global Variables** | **Notation** |
|---|---|
| Number of obligors | $n \in \mathbb{N}^*$ |
| Truncation parameter in the PCE | $M \in \mathbb{N}^*$ |
| Emission trajectory (e.g., SSP). Unit: $\mathtt{CO_2e}$ | $t \mapsto \widetilde{\gamma}_t$ |
| Atmospheric temperature trajectory | $t \mapsto \mathcal{T}_{\mathrm{ATM}}(t)$ |
| All energy sources available | $\mathscr{E}^{\mathrm{all}}$ |
| Discount factor | $r > 0$ |
| The reference time for the physical risk calibration | $t_{\mathrm{ref}}$ |
| Portfolio loss | $\mathcal{L}$ |
| Portfolio loss with rank-two PCA approximation | $\mathcal{L}^{\mathrm{PCA}}$ |
| Portfolio loss with rank-two PCA and PCE approximations | $\mathcal{L}^{\mathrm{PCA,PCE}}$ |
| Portfolio loss with rank-two PCA, PCE, and Gaussian approximations | $\mathcal{L}^{\mathrm{PCA,PCE,G}}$ |
| **Variables specific to the $i$th obligor** | **Notation** |
| Energy sources available | $\mathscr{E}^i$ |
| Vector of optimal GHG emissions at time $t$ | $\gamma^i_{\bullet,t} = (\gamma_{\mathtt{e},t})_{\mathtt{e} \in \mathscr{E}^i}$ |
| Optimal log production at time $t$ | $\widehat{p}^i_t$ |
| Optimal obligor's value at time $t$ | $\widehat{V}^i_t$ |
| Penalization and reward function | $\ell^i_1(\cdot)$ and $\ell^i_2(\cdot)$ |
| Penalty and reward coefficients | $\omega^i_1$ and $\omega^i_2$ |
| Systemic and idiosyncratic risk factors | $B$ and $B^i$ |
| Correlation to the systemic factor | $\rho^i$ |
| Average production level | $a^i$ |
| Mean-reverting parameter | $b^i$ |
| Dependence of the obligor's energy consumption on $\mathtt{e}$ | $c^i_{\mathtt{e}}$ |
| Average price | $\mathrm{AP}^i$ |
| Profit function | $\pi^i(\cdot)$ |
| Vector of prices per unit of all $\mathtt{e}$-energies consumed at time $t$ | $\alpha^i_{\bullet,t} = (\alpha^i_{\mathtt{e},t})_{\mathtt{e} \in \mathscr{E}^i}$ |
| | $\beta^i_{\bullet,t} = (\beta^i_{\mathtt{e},t})_{\mathtt{e} \in \mathscr{E}^i}$ |
| Vector of power/$\mathtt{CO_2e}$ ratio for all $\mathtt{e}$-energies. Unit: $\mathtt{kW/kgCO_2e}$ | $\theta^i_{\bullet,t} = (\theta^i_{\mathtt{e},t})_{\mathtt{e} \in \mathscr{E}^i}$ |
| Product of loss given default and exposure at default | $\Lambda^i$ |
| Poisson process associated to weather event $\mathtt{cw}$ and geographical zone $l$ at time $t$ | $N^{i,\mathtt{cw},l}_t$ |
| Corresponding Poisson intensity and loss | $\lambda^{i,\mathtt{cw},l}_t$ and $Z^{i,\mathtt{cw},l}_t$ |
| Expected physical loss at time $t$ | $\mathrm{EPL}^i(t)$ |
| Default barrier at time $t$ | $L^i(t)$ |

**Table 3** List of notations for the model parameters.


[3] Battiston, S., Mandel, A., Monasterolo, I., and Roncoroni, A. (2023). Climate Credit Risk and Corporate Valuation. *Available at SSRN 4124002*. https://papers.ssrn.com/sol3/papers.cfm?abstract_id=4124002.

[4] Bielecki, T. R., Crépey, S., and Jeanblanc, M. (2010). Up and down credit risk. *Quantitative Finance*, 10(10):1137–1151.

[5] Bourgey, F., Gobet, E., and Jiao, Y. (2024). Bridging socioeconomic pathways of CO2 emission and credit risk. *Annals of Operations Research*, 336:1197–1218.

[6] Bourgey, F., Gobet, E., and Rey, C. (2020). Metamodel of a Large Credit Risk Portfolio in the Gaussian Copula Model. *SIAM Journal on Financial Mathematics*, 11(4):1098–1136.

[7] Bourgey, F., Gobet, E., and Rey, C. (2022). A Comparative Study of Polynomial-Type Chaos Expansions for Indicator Functions. *SIAM/ASA Journal on Uncertainty Quantification*, 10(4):1350–1383.

[8] Calamai, P. H. and Moré, J. J. (1987). Projected gradient methods for linearly constrained problems. *Mathematical Programming*, 39(1):93–116.

[9] Carney, M. (2015). Breaking the tragedy of the horizon–climate change and financial stability. *Speech given at Lloyd's of London*, 29:220–230.

[10] Cormack, C., Donovan, C., Koberle, A., and Ostrovnaya, A. (2020). Estimating financial risks from the energy transition: Potential impacts from decarbonization in the European power sector. *Journal of Energy Markets*, 13(4).

[11] Cucker, F. and Smale, S. (2002). On the Mathematical Foundations of Learning. *Bulletin of the American Mathematical Society*, 39(1):1–49.

[12] EIOPA (May, 2022). European insurers' exposure to physical climate change risk : Potential implications for non-life business. *European Insurance and Occupational Pensions Authority Discussion paper*, EIOPA-22/278. https://www.eiopa.europa.eu/system/files/2022-05/discussion_paper_on_physical_climate_change_risks.pdf.

[13] Garnier, J., Gaudemet, J., and Gruz, A. (2021). The Climate Extended Risk Model (CERM). *Preprint arXiv:2103.03275*.

[14] Gatzert, N. and Özdil, O. (2024). The impact of dependencies between climate risks on the asset and liability side of non-life insurers. *European Actuarial Journal*, 14(1):1–19.

[15] Gómez, D. R., Wattersson, J., Americano, B., Ha, C., Marland, G., Matsika, E., Namayanga, L., Osman, B., Saka, J., and Treanton, K. (2006). Stationary combustion. *Energy, 2006 IPCC Guidelines for National Greenhouse Gas Emissions Inventories, Intergovernmental Panel on Climate Change, Geneva*. https://www.ipcc-nggip.iges.or.jp/public/2006gl/pdf/2_Volume2/V2_2_Ch2_Stationary_Combustion.pdf.

[16] Gordy, M. B. (2003). A risk-factor model foundation for ratings-based bank capital rules. *Journal of Financial Intermediation*, 12(3):199–232.

[17] Howard, P. H. and Sterner, T. (2017). Few and Not So Far Between: A Meta-analysis of Climate Damage Estimates. *Environmental and Resource Economics*, 68(1):197–225.

[18] International Energy Agency (2023). Emissions factors 2022. *IEA website*. https://www.iea.org/data-and-statistics/data-product/emissions-factors-2022.

[19] IPCC (2018). Summary for policymakers. In Masson-Delmotte, V., Zhai, P., Pörtner, H.-O., Roberts, D., Skea, J., Shukla, P., Pirani, A., Moufouma-Okia, W., Péan, C., Pidcock, R., Connors, S., Matthews, J., Chen, Y., Zhou, X., Gomis, M., Lonnoy, E., Maycock, T., Tignor, M., , and Waterfield, T., editors, *Global warming of 1.5 $^o$C. An IPCC Special Report on the impacts of global warming of 1.5 $^o$C above pre-industrial levels and related global greenhouse gas emission pathways, in the context of strengthening the global response to the threat of climate change, sustainable development, and efforts to eradicate poverty.* World Meteorological Organization, Geneva, Switzerland.

[20] Kenyon, C., Macrina, A., and Berrahoui, M. (2023). The carbon equivalence principle: methods for project finance. *Risk*.

[21] Kingman, J. F. C. (1993). *Poisson Processes*, volume 3 of *Oxford Studies in Probability*. The Clarendon Press Oxford University Press, New York. Oxford Science Publications.

[22] Krach, F., Macrina, A., Kanter, A., Hampwaye, E., Hlalukana, S., and Rateele, N. T. (2024). The Financial Impact of Carbon Emissions on Power Utilities Under Climate Scenarios. *International Journal of Theoretical and Applied Finance*, 27(01).

[23] Lando, D. (1998). On Cox Processes and Credit Risky Securities. *Review of Derivatives Research*, 2:99–120.

[24] Le Guenedal, T. and Tankov, P. (2024). Corporate debt value under transition scenario uncertainty. *Mathematical Finance*.

[25] Lefevre, A. and Tourin, A. (2023). Incorporating Climate Risk into Credit Risk Modeling: An Application in Housing Finance. *FinTech*, 2(3):614–640.

[26] Li, D. X. (2000). On default correlation: A copula function approach. *The Journal of Fixed Income*, 9(4):43–54.

[27] Malte, M., Nicholls, Z. R. J., Lewis, J., Gidden, M. J., Vogel, E., Freund, M., Beyerle, U., Gessner, C., Nauels, A., Bauer, N., Canadell, J. G., Daniel, J. S., John, A., Krummel, P. B., Luderer, G., Meinshausen, N., Montzka, S. A., Rayner, P. J., Reimann, S., Smith, S. J., van den Berg, M., Velders, G. J. M., Vollmer, M. K., and Wang, R. H. J. (2020). The shared socio-economic pathway (SSP) greenhouse gas concentrations and their extensions to 2500. *Geoscientific Model Development*, 13:3571–3605.

[28] McNeil, A. J. and Frey, R. (2003). Dependent defaults in models of portfolio credit risk. *Journal of Risk*, 6:59–92.

[29] Nesterov, Y. (2018). *Lectures on Convex Optimization*, volume 137. Springer.

[30] Nordhaus, W. and Sztorc, P. (2013). DICE 2013R Introduction and user's manual. *Yale University and the National Bureau of Economic Research, USA*. http://acdc2007.free.fr/dicemanual2013.pdf.

[31] Nordhaus, W. D. (1992). An optimal transition path for controlling greenhouse gases. *Science*, 258(5086):1315–1319.

[32] Olver, F. W. (2010). *NIST Handbook of Mathematical Functions hardback and CD-ROM*. Cambridge University Press.

[33] Özdil, O. (2025). A multi-period model for assessing the reinforcing dependence between climate transition and physical risks of non-life insurers. *The Journal of Risk Finance*, 26(1):98–121.

[34] Pachauri, R. K., Reisinger, A., et al. (2007). IPCC fourth assessment report. *IPCC, Geneva*, 2007:044023. https://archive.ipcc.ch/publications_and_data/ar4/wg1/en/ch2s2-10-2.html.

[35] Riahi, K., van Vuuren, D. P., Kriegler, E., Edmonds, J., O'Neill, B. C., Fujimori, S., Bauer, N., Calvin, K., Dellink, R., Fricko, O., Lutz, W., Popp, A., Cuaresma, J. C., KC, S., Leimbach, M., Jiang, L., Kram, T., Rao, S., Emmerling, J., Ebi, K., Hasegawa, T., Havlik, P., Humpenöder, F., Silva, L. A. D., Smith, S., Stehfest, E., Bosetti, V., Eom, J., Gernaat, D., Masui, T., Rogelj, J., Strefler, J., Drouet, L., Krey, V., Luderer, G., Harmsen, M., Takahashi, K., Baumstark, L., Doelman, J. C., Kainuma, M., Klimont, Z., Marangoni, G., Lotze-Campen, H., Obersteiner, M., Tabeau, A., and Tavoni, M. (2017). The Shared Socioeconomic Pathways and their energy, land use, and greenhouse gas emissions implications: An overview. *Global Environmental Change*, 42:153–168.

[36] Ritchie, H., Roser, M., and Rosado, P. (2022). Energy. *Our World in Data*. https://ourworldindata.org/energy.

[37] Roncalli, T. (2020). *Handbook of Financial Risk Management*. CRC Press.

[38] Schlömer, S., Bruckner, T., Fulton, L., Hertwich, E., McKinnon, A., Perczyk, D., Roy, J., Schaeffer, R., Sims, R., Smith, P., et al. (2014). Annex III: Technology-specific cost and performance parameters. In *Climate change 2014: Mitigation of climate change: Contribution of Working Group III to the fifth assessment report of the Intergovernmental Panel on Climate Change*, pages 1329–1356. Cambridge University Press. https://www.ipcc.ch/site/assets/uploads/2018/02/ipcc_wg3_ar5_annex-iii.pdf.

[39] Seneviratne, S., Zhang, X., abd W. Badi, M. A., Dereczynski, C., Luca, A. D., Ghosh, S., Iskandar, I., Kossin, J., Lewis, S., Otto, F., Pinto, I., Satoh, M., Vicente-Serrano, S., Wehner, M., and Zhou, B. (2021). Weather and climate extreme events in a changing climate. In Masson-Delmotte, V., Zhai, P., Pirani, A., Connors, S., Péan, C., Berger, S., Caud, N., Chen, Y., Goldfarb, L., Gomis, M., Huang, M.,

Leitzell, K., Lonnoy, E., Matthews, J., Maycock, T., Waterfield, T., Yelekci, O., Yu, R., and Zhou, B., editors, *Climate Change 2021: The Physical Science Basis. Contribution of Working Group I to the Sixth Assessment Report of the Intergovernmental Panel on Climate Change*, pages 1513–1766. Cambridge University Press, Cambridge, United Kingdom and New York, NY, USA.

[40] Vasicek, O. (1991). Limiting Loan Loss Probability Distribution. *KMV corporation.*

[41] Weitzman, M. L. (2012). GHG Targets as Insurance Against Catastrophic Climate Damages. *Journal of Public Economic Theory*, 14(2):221–244.